Challenges and Opportunities in the Development of Planar Potentiometric Sensors for Point-of-Care Analysis

Eliza J. Herrero and Philippe Bühlmann*

University of Minnesota, Department of Chemistry, 207 Pleasant St. SE, Minneapolis, Minnesota 55455, USA

Abstract: Despite decades of interest in the development of electrochemical point-of-care sensors, commercial applications are still hindered by unfulfilled needs. This review analyzes work in the field of miniaturized potentiometric devices, with a particular emphasis on reports from the past ten years. Research in this field has focused in particular on the types of underlying substrates to support these sensors, the degree to which sensing components are integrated into the substrate, the use of solid-contact materials to improve performance, and testing in real-life applications. This article highlights challenges in the design and performance of potentiometric point-of-care sensors that are preventing their wider use. Following an overview of differences in the layout of strip-type, sandwich-type, fully integrated, and fiber- and yarn-based sensors, the discussion focuses on the effects of materials and substrates on response slopes, potential reproducibility, and limits of detection.

Keywords: potentiometry, point-of-care, ion-selective-electrodes, paper-based, textile-based, ionophore

1 Introduction

Due to its excellent speed, sensitivity, and specificity, ion-selective potentiometry has been for several decades the method of choice for the measurement of ions and charged biomolecules in clinics [1]. Given the high interest in miniaturized point-of-care electrochemical sensors, it is not surprising that many efforts have been made to adapt the design of ion-selective electrodes (ISEs) for point-of-care usage [2–8]. In contrast to traditional ISEs, these sensors are characterized by a low dimensionality and the requirement of an underlying support substrate to support the electrochemical cell. The earliest examples include commercially available clinical blood analyzers designed for use outside of centralized laboratories, such as the Kodak Ektachem benchtop analyzer of the early 1980s[9] and the i-Stat portable clinical blood analyzer introduced into hospitals in the early 1990s [10]. They brought clinical chemistry testing to patient bedsides by replacing the conventional rod- or tube-shaped electrodes with slides or cartridges.

Notably, the commercial impact of these sensors is still limited. The ASSURED criteria (Affordable, Sensitive, Specific, User-Friendly, Rapid, Robust, Equipment-Free, and Deliverable to end user) for point-of-care diagnostics, as put forth by the World Health Organization (WHO), present a framework to assess the cause for the limited commercial availability. Only devices that meet most of these criteria can truly function as point-of-care devices and, thereby, have the potential to make it to market [11,12]. Affordability of a device in production is often difficult to assess from academic settings but worth consideration nonetheless [13]. Performance-related criteria, such as sensitivity, specificity, and speed of analysis, depend upon the particular sensing mechanism chosen

as well as performance limitations that arise in miniaturization. Meeting the “user-friendly” criterion requires that use of a device is limited to a maximum number of steps that an untrained user can readily perform. Ideally, this includes a calibration-free design, a difficult feat that has attracted much recent attention [14,15]. In addition to testing device performance in the laboratory, field testing is needed to allow for optimization in realistic settings of use by non-trained personnel, as a recent report of a case study for a colorimetric test development highlights [16]. The design of an ISE that complies with the ASSURED criteria is difficult, as there are often tradeoffs in device design and analytical performance.

There is no single term that can be readily used to describe miniaturized sensors designed for point-of-care usage. While the term point-of-care is quite well-known and, at times, even misused, searches of the literature that are based on a straightforward combination of keywords (such as, e.g., point-of-care, potentiometric, miniaturized, microfluidic, portable, two-dimensional, and wearable) not only fail to provide a list of all relevant work but also yield a large number references that are out of scope. This makes it difficult in particular for newcomers and those working outside of this discipline to understand the full extent of activities in this field. This is in fact one of the motivations for the present article.

Recent reviews have surveyed the development of wearable potentiometric sensors for clinical use [6] or the use of electrochemical sensors in general [18]. Others have focused on the field of paper-based sensors, highlighting fabrication methods for paper-based electrochemical sensors [17], devices using paper as a supporting substrate for potentiometric devices [7], or the use of textiles in electrochemical devices [8]. In

emphasizing a single substrate, these previous reviews do not provide the detailed comparison of the effects of different substrate materials on device performance as attempted in this review .

This review discusses research on the design, fabrication, and performance of ISEs for point-of-care usage. We begin with an overview of common sensor designs, categorized by the degree of miniaturization of the sample holder, reference electrode (RE), and ion-sensing electrode, as summarized in Figure 1. Miniaturized potentiostats, displays integrated into ISE devices, and chemically sensitive field-effect transistors are out of scope and will not be considered. We then introduce common materials that have been used as the underlying support substrate upon which miniaturized ISEs are fabricated, with an emphasis on their physiochemical characteristics. We then examine how the sensor design and identity of the supporting substrate affect deviations of the sensor performance from ideal behavior. In particular, response slopes, reproducibilities, and the lower limits of detection of miniaturized ISEs are compared to those of analogous conventional rod- or tube-shaped ISEs. In critically analyzing the performance limitations correlated with design and material choices, this review serves as a guide for the further improvement of miniaturized potentiometric devices.

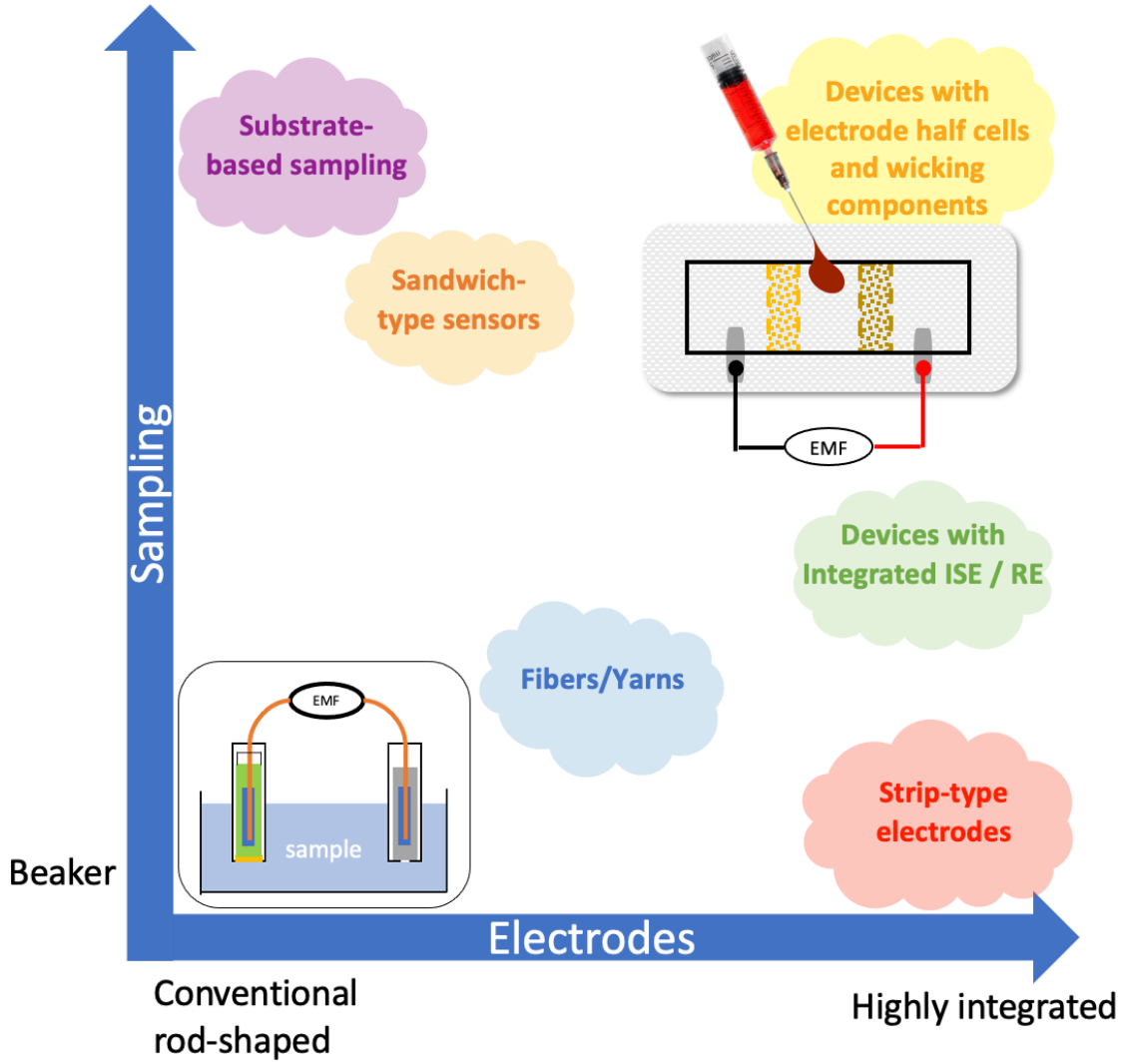

Figure 1. Categories of miniaturized potentiometric sensors, organized according to the level of integration of sampling and the sensing electrode(s).

2 Strategies for the design of miniaturized potentiometric sensors for point-of-care usage

2.1 Substrate-based sampling

In substrate-based sampling, a sample is wicked across a single-use hydrophilic substrate in contact with traditional rod-shaped ISEs and REs (see Fig. 2A). Such

substrates include various types of papers, textiles, and sponges (see Section 3 of this review). This design was originally introduced as a dot-blot assay with two vertically oriented conventional rod-shaped electrodes; one electrode upside down and the other right side up, with filter paper sandwiched in between them. A drop of sample was deposited onto the paper, resulting in wicking of the sample into contact with the electrodes [19]. A very similar approach involves two horizontally oriented electrodes, with the upper part of a piece of filter paper sandwiched between the electrodes and the lower part of the filter paper dipped into the sample below [20].

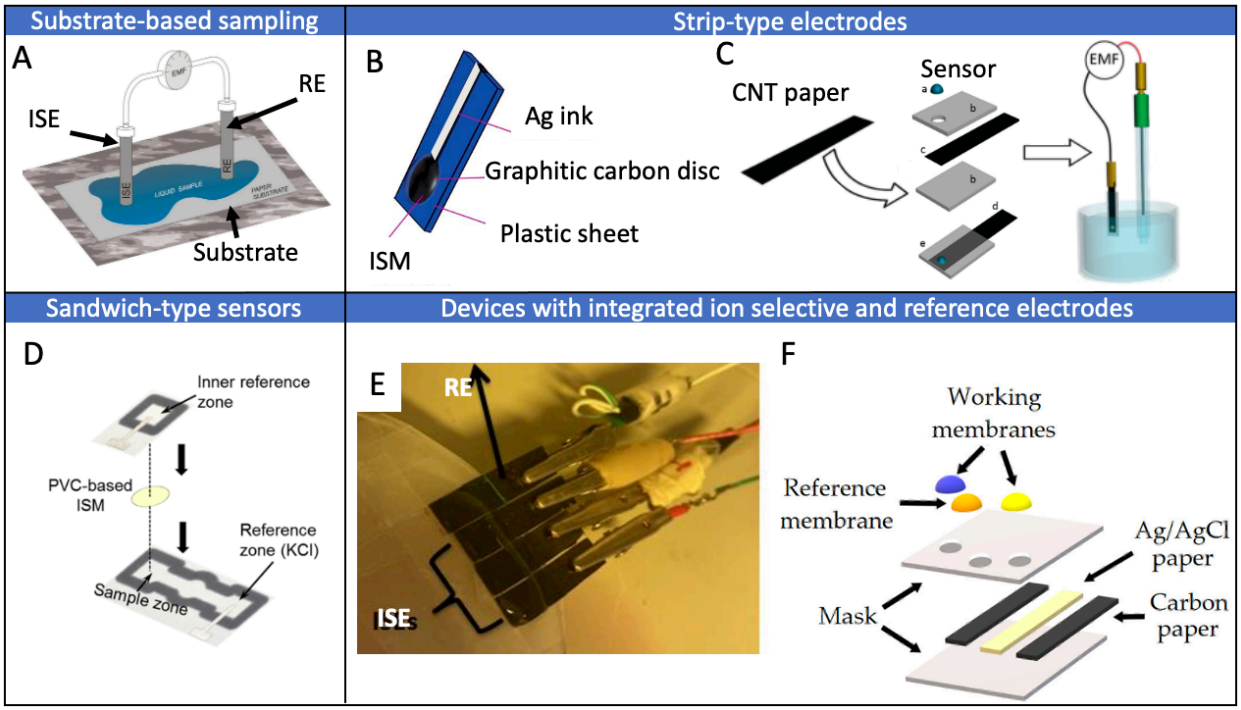

Figure 2. Design of ISEs for point-of-care analysis: (A) substrate-based sampling, (B) strip-type electrodes with the solid-contact restricted to the lower portion of the strip, (C) strip-type electrodes with the solid-contact entirely covering the entire substrate, (D)

sandwich-type devices, as well as (E) and (F) devices with both an ISE and RE. Adapted with permission from references **[21–26]**, respectively.

An alternative mode of substrate-based sampling includes two vertically oriented electrodes clamped into place, as shown in Fig. 2A [21,27–34]. Further, the conventional single-junction RE was replaced by a reusable Ag/AgCl rod and a disposable salt bridge [35]. For the latter, a separate piece of filter paper was coated with dry KCl and placed between the Ag/AgCl rod and the filter paper containing the sample. This isolates the electrode from contact with, and thereby fouling by, the sample. In addition to reducing the required sample volume to 200 μL, substrate-based sampling also filters off particulates from samples such as soil and sludge, which has been argued to harm electrodes in traditional sampling [21,30–32]. The use of conventional ISEs in all these cases necessitates a trained user to frequently re-calibrate the ISEs.

2.2 Strip-type electrodes

Strip-type electrodes use the underlying substrate to physically support the device but they do not hold the sample. Electrodes are built vertically on top of a substrate by application of a conductive lead, solid contact, polymeric membrane, and an insulating mask onto the substrate (Fig. 2B). The substrate is often filter paper, and the mask prevents samples from directly contacting the conductive lead. The sensor is connected to a potentiostat through the conductive leads and is submerged into the sample, typically along with a conventional RE [2,4,22,23,36–39]. While these sensors can be referred to as disposable, they are reusable and can be rinsed between samples.

The earliest strip-type ISEs used a coated-film design in which a film of the polymeric sensing membrane was deposited on top of Ag-coated filter paper [2]. However, when an ion-selective membrane (ISM) is directly placed onto a conducting metal, the interface between these two materials is typically blocked with respect to charge transfer. Consequently, the phase boundary potential at this interface is not well defined, resulting in poor potential stability and reproducibility unless surface oxidation can be prevented and a high surface area provides a large interfacial capacitance [14]. Therefore, subsequent devices of this type were designed with solid contacts such as conducting polymers [36] and, later, with high surface area contacts with a high capacitance [23,37,38,40].

Strip-type ISEs in which filter paper is fully coated with carbon nanotubes (CNTs) have been fabricated (see Fig. 2C) [23,37,38]. This inherently uses a rather large amount of solid-contact material but does not require the use of a stencil or detailed deposition of ink. In contrast, in most strip-type sensors the solid-contact material is restricted to the area directly underneath the ISM and does not extend all the way to the wires that connect the device to a potentiometer. Instead, a separate path of an electron conducting material is provided on the device to connect the solid-contact material to external wires (see Fig. 2B). These conductive paths are commonly applied by screen-printing.[41] Alternatively, they can be drawn with a 3D pen [39], as first shown with ion-sensing pencils.[42] Such strip sensors have been used in many settings, including in-vitro monitoring of drug release from solid-dose pharmaceuticals, which offers a real-time alternative to off-line HPLC testing [22],

While strip-type sensors have typically been used for measurements in samples of large volumes, this does not need to be the case. Smaller sample volumes are conceivable so long as the liquid junction of the RE is covered with sample solution. Notwithstanding, the use of strip-type sensors in point-of-care settings is impeded by the need for a conventional RE, an insulating layer, and sample volumes large enough to dip the electrodes into. Therefore, strip-type sensors may best be seen as stepping stones towards fully integrated devices.

2.3 Devices with integrated ion sensing and reference electrodes

Moving towards more integrated devices, many groups have fabricated both reference and sensing electrodes onto the same unit. As in strip-type sensors, these devices use the underlying substrate solely as a physical support, and the sample is not contained in any part of the device. Such devices require manual application of the sample directly to the sensing elements or submersion of the device into a sample. As with strip-type sensors, they are reusable and can be rinsed between measurements of different samples.

A crucial step in the preparation of such devices is the fabrication of planar REs. Common solid-contact REs include CNT-coated paper onto which a reference membrane comprising an ionic liquid has been applied [25,43,44], graphene/multiwalled CNT coated substrates in contact with a reference membrane containing AgCl and a hydrophilic electrolyte (such as KCl or NaCl) [45–47], as well as AgCl/Ag coated filter paper in contact with a poly(vinyl butyral) membrane doped with NaCl and $AgNO_3$[48].

To include reference and sensing electrodes in a single unit, separately prepared strip-type ISEs and REs can be paired [25,43,48]. This has been accomplished by taping

a rubber spacer between strip electrodes to form a cavity for sample introduction,[43,48,49] as well as by taping strip electrodes together, side by side, to form a flat array (see Fig. 2F) [25,44]. In a notably efficient design, three separate strips of conductive material were sandwiched between plastic masks, and then ISMs and reference membranes were deposited onto pre-cut holes to form an array of sensing electrodes and REs (see Fig. 2E) [26]. Fabrication is simplified by the use of a single piece of supporting substrate as the base for both the sensing and reference electrodes.

Screen-printing or spray-coating of conductive leads and/or solid contacts in combination with drop-casting of membranes by hand has been repeatedly reported for the quick fabrication of integrated sensors, as mentioned above for strip-type sensors too. For example, poly(ethylene terephthalate) (PET) substrates were coated with single-walled carbon nanotubes (SWCNTs) as solid contact, followed by screen-printing to deposit both ion-selective and reference membranes [40]. Similarly, to form an ISE array, graphene was deposited onto a paper substrate using spray coating with a stencil.[46] Also, a Chinese brush pen was used to “write” graphene leads followed by polymeric membranes onto a PET substrate [47]. In an even more integrated system, a 3 wirelessly controlled robot with 3D-printed housing parts was used to deposit carbon black, both ion-selective and reference membranes, and even the conditioning solution on a PET substrate [50].

Screen-printed ISEs have been coupled with miniaturized integrated circuit boards and used for on-body detection of glucose, lactate, Na^+, and K^+ in sweat [51,52]. These devices were used as patches that are directly applied onto skin to detect these analytes in sweat, but there are questions as to how old sweat is replaced by fresh sweat.

While these sensors represent a step towards integration, they are limited for use with real samples by the lack of a wicking component. The electrodes must be dipped into samples, as typical for strip-type electrodes, or the samples must be deposited onto the sensing membrane.

2.4 Sandwich-type sensors

Sandwich-type designs, in which a free-standing sensing membrane is placed between two pieces of filter paper, combine both the reference and sensing elements into the device and have the inherent wicking capabilities of the underlying support substrate (see Fig. 2D). The free-standing membrane may be reused for multiple measurements, but the filter paper onto which the sample and reference solutions are deposited needs to be replaced for each measurement.

The reference element in these sensors is based off a paper-based design introduced originally in the context of voltammetric sensing [53]. It consists of wax barriers in a dumbbell shape to define reference, sample, and central contact zones, with a strip of Ag/AgCl ink in the reference and sample zones. These sensors are produced by ink-jet printing of wax barriers, followed by heat exposure to ensure penetration of the wax into the substrate, as is common for the fabrication of hydrophobic barriers on filter paper.[54,55] Upon placement of a solution with a known KCl concentration on one side of the dumbbell shaped region of the filter paper, the device can be used as a Cl^- ISE [53].

The first combination of devices of the above type with an ISM was achieved by clipping a free-standing ISM between a filter paper reference half cell and a filter paper half cell onto which the sample was deposited [24]. This design was used both with

ionophore-free ion-exchange membranes[24,56] and ionophore-doped ISMs [24]. Fabrication of sandwich-type designs was subsequently simplified by 3D printing of an ISM onto a selected area of a single piece of filter paper, followed by folding of the paper onto itself, avoiding the use of three distinct parts as used in the original design [57].

2.5 Planar devices that comprise both electrode half cells and wicking components

Combining all sensing components and the ability to wick the sample into a single (unfolded) piece of supporting substrate is a promising approach to simplify the fabrication and handling by the end user. This can be achieved by use of a hydrophilic support material with inherent wicking capabilities and by integration of the membranes into the material itself.

By depositing both the sensing and reference membranes onto the filter paper and using Ag/AgCl ink in contact with a KCl solution as a reference half cell, the number of parts of entire Cl^- and K^+ sensing devices was reduced from three [24] to one (see Fig. 3A) [58]. This design was subsequently also utilized in combination with textile substrates [59]. Use of these devices requires deposition of one droplet of reference solution to each of the two reference zones, and one droplet of sample to the sample zone. While these devices use a single piece of material to contain both electrodes as well as the sample and reference solution, they still require the application of an inner filling solution, adding steps that the end user must perform.

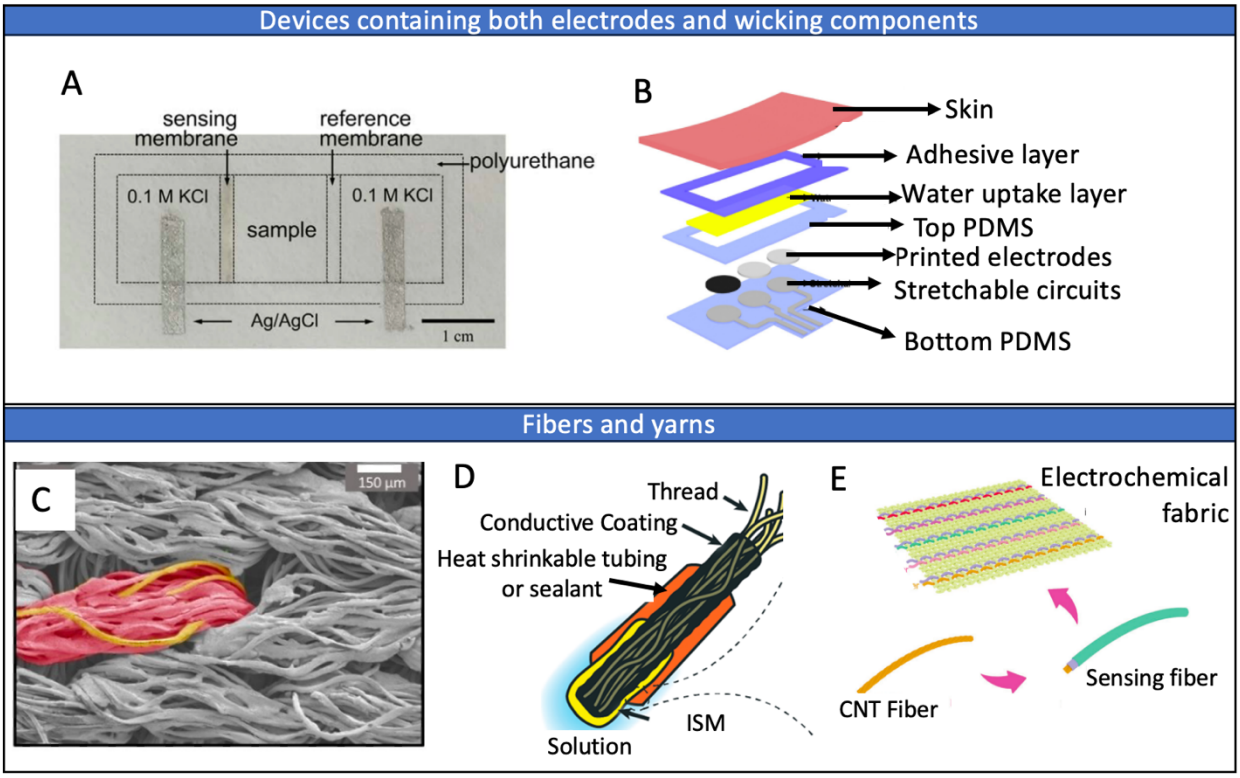

Figure 3. Examples of (A) miniaturized potentiometric sensing devices with both the sensing and REs as well as sample-wicking components integrated into the support substrate, and (B) devices containing integrated reference and sensing electrodes with a separate sample-wicking component. (C) Scanning electron microscopy image of a fabric, with a single yarn highlighted in red and individual fibers in yellow. (D) Thread-based ISE and (E) thread-based ISEs woven into a piece of fabric. Adapted with permission from references **[58–62]**, respectively.

This design can be further optimized through replacement of the inner filling solutions with a solid contact, as this has also been shown for many screen-printed ISEs. A proof-of-concept for a fully integrated solid-contact RE was made by the application of a colloid-imprinted mesoporous carbon doped with a hydrophobic redox couple placed

between Ag/AgCl ink as the inner reference element and an ionic-liquid-based reference membrane for direct contact with the sample [63]. Colloid-imprinted mesoporous carbon was also used to interface a hydrophilic high-capacity anion-exchange membrane for Cl^- detection with its own inner Ag/AgCl ink RE [64]. While in this case all components were applied by hand with a micropipette, inkjet printing was used for fully integrated devices comprising a Ag/AgCl/KCl/reference membrane RE and an ISE prepared with graphene, poly(3,4-ethylenedioxythiophene) (PEDOT) doped with polystyrene sulfonate (PSS), and an ionophore-doped ISM [65]. The end user of such a fully integrated solid-contact device only needs to apply the sample (10 or 20 µL, respectively); upon connection to a voltmeter, a stable signal is reached within 30 s.

While most sensors of this type were designed in view of samples available in droplet form, this type of integrated design is also amenable to wearable devices. For example, for on-body readout with a wearable potentiometer, a microfluidic sensor was fabricated on a cotton T-shirt by infusing the shirt with poly(acrylonitrile-*co*-butadiene-*co*-styrene) to form hydrophobic barriers, followed by screen-printing of ion-selective and reference membranes for Ca^{2+} detection [66]. In addition to introducing a novel, scalable approach to creating hydrophobic barriers on textiles, this report also demonstrated the need for microfluidics to refresh sweat in detection zones by comparing errors in devices with and without a microfluidic patch to refresh the sweat.

In some devices without integrated sample-containing capabilities, additional elements can be attached to enable samples to flow to or across electrodes. In one fully reusable device, in order to move sample solution from the inlet well into contact with sensors, a piece of filter paper was incorporated into a thermoplastic unit with a built-in

ISE and RE.[67] For another example, a separate microfluidic cell was 3D-printed and coupled with a screen-printed electrode to ensure old sweat samples were replaced by new ones, enabling on-body sweat measurements [68]. On-body patches for measuring concentrations in sweat have also been fabricated with sponges [60] and filter paper [69] as sample recipients (see Fig. 3B). Sweat was also wicked into contact with ISEs and REs printed onto a single piece of PET coupled into a custom-built smart watch for immediate and local reading of results [70]. Evidently, designs of this type are more complex to fabricate.

2.6 Fibers and Yarns

Within the field of textile-based sensors, there is no uniform consensus on the use of the terms fiber, thread, and yarn. For clarity, we define here the terms as we use them throughout this review. A fiber is defined as the smallest base unit of a textile; a thread is a thin single strand of fibers, as used in sewing and embroidery; and yarn is a thick strand of fibers used in knitting and crocheting (see Fig. 3C for examples of yarn and fibers). Electrodes have been made from all three.

Threads have been coated with conductive inks and ion-selective membranes by either dip-coating [71] or application with swabs or brushes [61], resulting in diameters of the coated threads of 1 mm or less (see Fig. 3D). Cross-sectional images confirm an external coating of threads but show that there is no penetration of the polymeric membrane into the inter-fiber space below the thread surface [61,71]. As the strip-type ISEs mentioned above, thread-based ISEs too have been used by immersion into samples, with small sample volumes as a major benefit. For example, several thread-based ISEs with selectivities for different ions and diameters of 600 µm were coupled

together for multiplex sensing in sample volumes as low as 200 µL [61]. A thread-based RE was also developed, making fully miniaturized potentiometric thread-based devices possible [71,72].

Thread-based ISEs have also been incorporated into devices that contain a wicking component, expanding the applications of these sensors to uses without a separate sample holder. For example, for continuous sensing of wound pH, a cotton yarn based ISE coupled with a commercial mini-RE was attached with heat shrinking tape to a band-aid [73]. Thread-based ion-selective and REs were also glued into an on-body patch that contained a cotton strip to wick sample into contact with threads [74].

Threads have been reported to maintain high flexibility and mechanical strength when used for ISEs, which allows them to be sewn/woven into textiles (see Fig. 3E) [62,75,76]. For example, for sweat monitoring, thread-based ISEs and an RE were sewn into a bandage, held in place by a hydrophobic adhesive film, and covered with a strip of absorbent gauze to wick sweat across electrodes.[76] The absence of glues and adhesives in contact with ISEs is desirable, both to simplify the fabrication and to remove potential sources of contamination. For example, sensing and reference fibers were directly woven into a fabric [62]. Thereby, the sensing fabric maintained structural integrity despite bending, twisting and rinsing, while screen-printed electrochemical textiles often suffer delamination under similar conditions [62].

Fiber-based electrodes are much smaller than thread-based electrodes and often require a 2-step integration for incorporation into textiles. For example, Au nanowires with ISM or reference membrane coatings, with final diameters of 500 µm, were wound around a length of spandex, which was then integrated into a headband [75]. Also, potentiometric

sensors prepared with microfibers prepared from reduced graphene oxide were braided into a silk fiber and then sewn into a t-shirt [77] .

3 Materials and substrates used

3.1 Guiding principles

To meet the demands for a point-of-care device, materials used as supporting substrates must meet several criteria. A minimum of mechanical strength is necessary if devices are to be transported to and used in field settings, but the material does not need to be as robust as for wearable devices. For large scale production, all fabrication steps must be compatible with mass-production methods, replacing the manual assembly typical in research. The supporting substrate must be inert towards both sample and sensing components and cannot negatively affect the analytical performance. Acceptable options include materials whose surface chemistry can be easily altered to meet these criteria. Ready availability and low cost are important [11,78]. To fabricate devices with the ability to contain samples and control fluidic flow, substrates must be compatible with methods that allow the formation of hydrophobic channels or other types of barriers, as they can be obtained, e.g., by wax-printing or laser cutting. For a fully integrated device that moves samples from a sample introduction zone into contact with sensing components, the substrate material must have wicking abilities, and the sample uptake, evaporation speed, and wicking rate must all be considered.

A thorough characterization of such substrates is important to identify early on possible interactions with samples, contaminants, and additional information necessary to understand performance limitations, as discussed in Sections 4-6 below. When using

materials purchased from companies that provide online databases and material safety data sheets, authors of research publications often include little characterization information as they assume that readers can look up relevant information online. However, information available on-line may not reflect changes to commercial products over the years, and it may not be available to future readers. Moreover, information supplied by manufacturers is often limited for proprietary reasons. Therefore, we recommend that authors list in publications as much data from materials safety data sheets as well as other information from suppliers as available to them. Moreover, many publications refer to supporting substrates as purchased from “local stores,” providing readers little opportunity to obtain additional information. In such cases, it is particularly important for authors to report a full physiochemical characterization of all materials used.

3.2 Polymeric supports

One broad category of supports used for miniaturized potentiometric devices are non-porous synthetic polymeric materials that serve only as a physical backing and support. PET, an economical thermoplastic polymer of high tensile strength that can be spun into textiles or extruded as a hard plastic [79,80], is one of the most common synthetic polymers used. It has been used for the preparation of ISEs as sheets [4,40,47,69,70,81] and films [51,52] of various thicknesses (see Fig. 4A). Other nonporous polymeric substrates used as supports for ISE devices include a polyimide [82]polyurethane (in this case with full details on in-house preparation and characterization) [68], polydimethylsiloxane[60], 3D-drawn polylactide[39], and polypropylene paper [45].

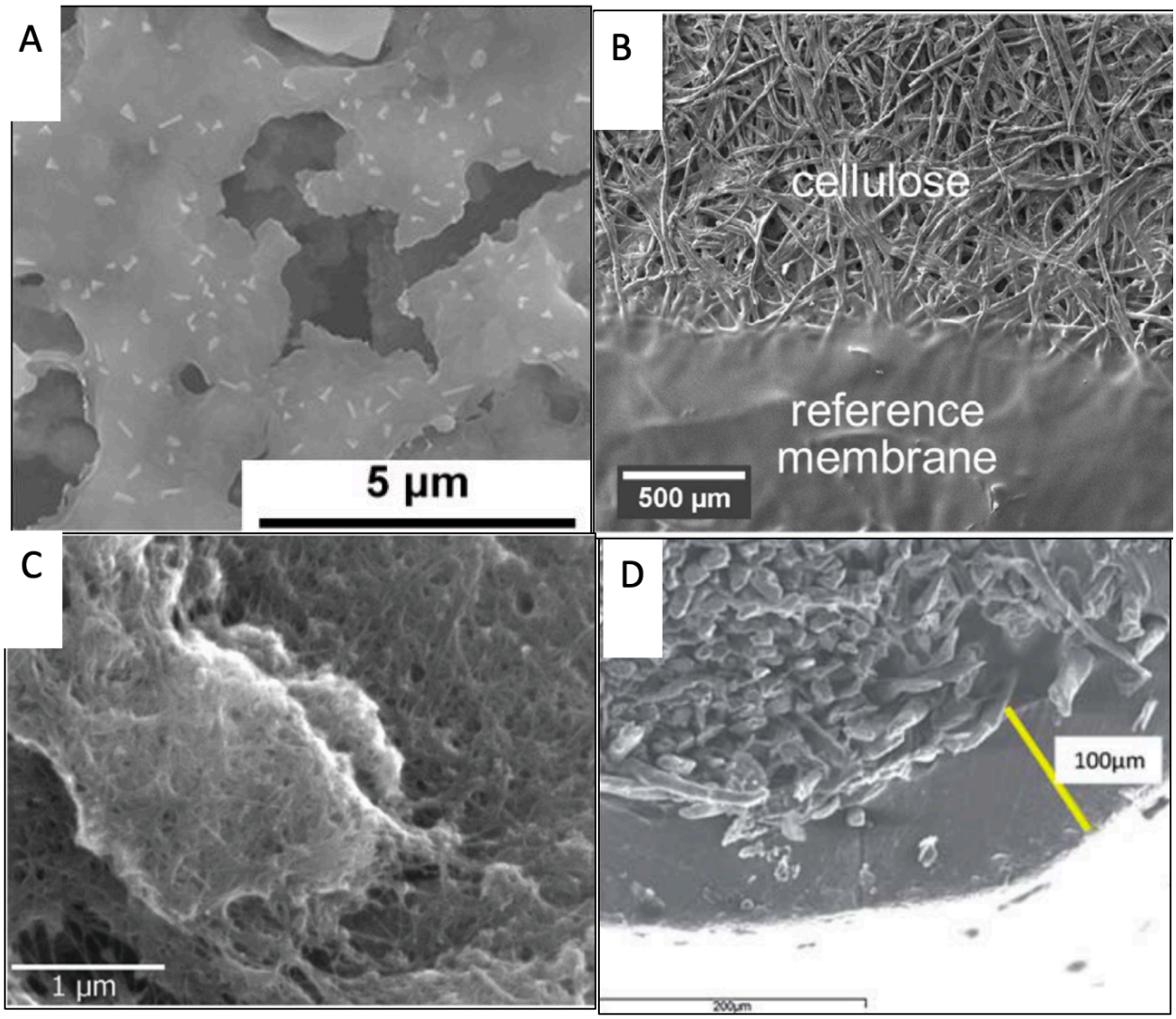

Figure 4. Scanning electron microscopy images of coated substrates: (A) NaCl doped poly(vinyl butyral) reference membrane deposited on top of a sheet of PET, (B) ashless filter paper coated with a PVC reference membrane, (C) CNT coated filter paper, and (D) cross-sectional view of a membrane coated yarn. Reproduced with permission from references [23,52,58,83], respectively.

3.3 Paper

Filter paper, composed of randomly oriented alpha cellulose fibers, is another very common material used in point-of-care devices due to its high mechanical stability, wicking abilities, bio-degradability, and, when purchased in bulk quantities, low cost [2,7,9,84–86]. The use of wax printing to quickly print hydrophobic barriers to control fluid flow, as shown first in 2009 [54,55], has greatly increased paper's popularity.

As filter papers have been traditionally used for many separation and purification processes, they are available in many pore sizes and ash contents. Devices have been made with qualitative filter paper of 11 μm pore size (Whatman 1, ash 0.01%)[24,56] as well as ashless quantitative filter papers with pore sizes of 12-25 μm (Whatman 589/1, Black-Ribbon) [20,21], 4-12 μm (Whatman 589/2, White Ribbon) [20,58,63,64], and 2 μm (Whatman 589/3, Blue Ribbon)[21] (see Fig. 4B). Nitrocellulose paper with a pore size of 0.2 μm was also used [19]. While filter paper is the most common type of paper used in potentiometric devices, other cellulose-based materials such as tissues and delicate task wipes have also been used for substrate-based sampling [21].

Filter paper has also been modified in a variety of ways to minimize interactions with analytes, enhance ease-of-use, or create highly conductive surfaces. Because the negatively charged cellulose may interact with samples (see Sections 4-6), the surface of cellulose filters has been modified through exposure to acid solutions [31], inorganic salts [28], and ISM components (i.e., PVC, the plasticizer 2-nitrophenyl octyl ether, the ionic site potassium tetrakis(4-chlorophenyl) borate, and the Pb^{2+} ionophore *tert*-butylcalix[4]arene-tetrakis(*N,N*-dimethylthioacetamide)) [29]. Modifications to improve the sensors' ease-of-use, such as protamine-doping to enable ionic-strength independent

measurements [34] and Au-modified filter paper to reduce biofouling of conventional sensors by blood [27], have also been reported. Paper has been saturated with KCl to serve as a pseudo-RE [35,65] and fully coated with inks based on CNTs (see Fig. 4C) [23,37,38,43,44], carbon, and AgCl/Ag[26] to serve as conductive leads. Finally, paper has also been fully functionalized with a silylation reagent with terminal perfluoroalkyl groups and coated with carbon nanotubes or graphene to create a highly hydrophobic, conductive substrate upon which electrodes were printed [46,49].

While such modifications enhance overall device performance, some of these fabrication steps eliminate the unique hydrophilic character of paper, add significant cost and fabrication complexity, and compromise the biodegradability provided by paper. In some cases, one may wonder whether the unique attractiveness that comes along with a “paper-based” device still applies, and whether the use of paper is indeed justifiable.

3.4 Textiles

While textile-based sensors are commonly known for use in wearable devices, many of the characteristics that make them well-suited for wearable devices also make them attractive for miniaturized sensors for point-of-care usage [8,87]. These include high flexibility, robustness, and ease of control of physical dimensions.

A variety of non-conductive textiles have been used as supports for miniaturized sensors, with cotton and polyester the most common ones. As a naturally derived material, cotton is generally seen as more sustainable and more easily disposable than synthetic materials. Cotton has been used in the form of thread (see Fig. 4D) [61,71,83], a 0.3 mm thick shirt [66], textile samples purchased from local clothing stores (without further description) [32,88], and as a blend with 5% elastane [32]. As similarly mentioned

earlier in this review, a lack of additional details on the composition or physical properties of these materials limits a thorough analysis of the effect of substrate properties on device performance.

Polyester is the most commonly used synthetic material for textile-based sensors and has been used in the form of threads [76], a cleanroom wipe [59], apparel purchased from local clothing stores (without further description) [32,88], as well as polyester textiles blended with 5% elastane [32] or coated with polyurethane [88]. While PET is the most common form of polyester used in fiber production [89], it cannot be assumed that all commercially available polyesters are only made from the same monomers as PET. If the identity and purity of a particular polyester, polyamide, or polyurethane is in question, a simple alkaline hydrolysis of the material may be performed to isolate the monomeric units for analysis [59]. Analysis by infrared spectroscopy provides an alternative nondestructive alternative, but it is less likely to help in the identification of minor components. Polyimide, as well as polyimide-elastane blends have also been used in substrate-based sampling [32].

Threads composed of conductive fibers offer not only mechanical robustness but also eliminate the need to apply a conductive coating, which has resulted in their increased popularity. Lab-made conductive fibers synthesized and incorporated into potentiometric sensors include lab-spun CNT fibers,[62] Au nanowires, styrene-ethylene/butylene-styrene fibers [75,90], and reduced graphene oxide fibers [77]. While in-house fabrication offers a better control of the fiber properties, ready availability is another key property that should be considered when evaluating possible supporting substrates. In an effort to address this concern, commercially available conductive carbon

fiber threads (1 mm ∅ with 6 µm ∅ fibers [74] and 0.27 mm ∅ with 0.08 mm ∅ fibers [71]) and stainless-steel fibers [76] have also been used. While commercially available conductive threads simplify the fabrication of sensors, they still cost significantly more than non-conductive materials.

Each material offers distinct advantages and disadvantages that must be evaluated in the context of the specific use and device design. An important factor that must be considered in every case is the potential interaction of the material with sample or sensing components—interactions that can alter the device performance and are examined in the following sections in view of their effect on the response slope, potential reproducibility, and lower limits of detection of potentiometric sensors.

4 Effects of materials and sensor design on response slopes

4.1 Response slopes in potentiometry

The measured potential as measured with an ISE, often referred to as the electromotive force (EMF), is a function of the activity of the target ion in the sample. It is described by the Nernst equation, $EMF = E^0 + 2.303RT/(z_iF)\log a_i$, where R, T, z_i, F, and a_i represent the universal gas constant, temperature, ion valency, Faraday's constant, and activity of the target ion i with charge z_i, respectively [91]. At 20 °C, this results for the plot of EMF versus log a_i in a linear response with a slope of 58.2 mV z^{-1} / decade, which is referred to as a Nernstian response.

Arguably, the response slope of an ISE should be referred to as non-Nernstian when the value of the Nernstian slope falls outside of the confidence interval determined from a fit of the experimental data. However, the literature often only reports slope values,

even though standard deviations or confidence intervals would be readily available from such fits. Therefore, we refer in this review to distinctly sub- or super-Nernstian response slopes when a reported response slope deviates by $6\ \mathrm{mV}\ z^{-1}$ / decade or more from the theoretical response slope. In the absence of a widely expected criterion for when a response slope deviates significantly from theory, we chose this admittedly arbitrary value because it corresponds to a >10% deviation from the theoretically predicted Nernstian slope. When standard deviations are reported, response slopes within standard deviation of this range are also considered Nernstian. While a sensor with a linear but non-Nernstian response slope can still be used to make accurate determinations of target ion activities, it is important to understand the source of non-theoretical responses to assess the robustness of a device. Too often, a non-theoretical response slope also comes along with limited reproducibility.

4.2 Common sources of non-theoretical slopes

In reviewing response slopes for miniaturized devices as reported in the literature, we noticed three common origins of non-ideal performance: improper calculation of response slopes, response slopes computed using data outside of the Nernstian range, and interactions between target ions and underlying support substrates.

When two electrolyte solutions contact each other, as at the interface of a sample and a bridge electrolyte that separates the sample from a RE, a liquid junction potential arises. If this liquid junction potential varies over the range of the calibration curve, the response slope deviates from the expected theoretical (Nernstian) value. In many cases, this can be avoided by correcting for the liquid junction potential using the Henderson equation [91]. Similarly, if activity coefficients vary with the sample composition, plots of

the EMF versus the logarithm of the sample concentration will give nonlinear response slopes. This can be avoided by converting the concentration of the target ions to activities, which can be achieved, e.g., by using a two-parameter Debye–Hückel approximation [92]. Many readers will find this obvious, but we note that there are quite a number of reports in the literature that do not account for either liquid junction potentials or activity coefficients [28,29,31,35,45,49,52,60,61,65,82].

While most of slope deviations of this type are smaller than the $6\ \mathrm{mV}\ z^{-1}$/ decade tolerance defined above, they are still an important factor to consider when evaluating the literature. For example, when using a RE with a 3 M KCl solution contacting samples comprising 1–100 mM KCl, the slope of the Cl^- response will decrease by 0.4, 3.6, or 3.9 mV/decade when failing to account for liquid junction potentials, activity coefficients, or both liquid junction potentials and activity coefficients, respectively. For the same RE in a sample of 1–100 mM $CaCl_2$, the respective Ca^{2+} slopes will increase by 1.0, 2.1, and 3.0 mV/decade.

The second pattern observed in reports of non-ideal slopes for miniaturized potentiometric devices is that of poorly chosen activity ranges for linear fits. If a linear fit is chosen past either the upper or lower LOD, it will be skewed by data points that are not in the linear sensing region of the ISE, resulting in an artificially high or low slope. Visual inspection of a calibration curve will often reveal such errors [51,52,76].

The third major source of non-ideal slopes as reported for miniaturized ISEs can be explained by interactions between target analytes and the underlying support substrate of the sensor device. The most common example for this is binding of divalent cations to filter paper or wood fibers, an error that correlates with the strength of

interaction between these ions and the underlying support [21,35]. A super-Nernstian jump in the lower concentration range has also been observed [28], similar to that seen in either unconditioned membranes or samples with ion fluxes towards the inner filling solution [93]. In attempts to mitigate the effect of substrate interactions with target analytes, thoughtful work has compared the performance of sensors built from different supporting materials, resulting in suggestions on material choices to improve response slopes, response times, and lower detection limits [30,32].

4.3 Slopes in substrate-based sampling

Super-Nernstian responses have been reported for devices with substrate-based sampling in either the full or lower concentration ranges. For a solid-contact RE and a solid-contact K^+ ISE used with filter paper-based sampling, the pore size of the filter paper was shown to correlate inversely with the slope. A slope of 63.1 $\pm$ 5.8 mV/decade was found for paper with 2 μm pores in contrast to 54.7 $\pm$ 2.1 mV/decade for paper with 12-25 μm pores. Additionally, when varying the shape of the sampling substrate, the response slope as obtained with filter paper with larger pores was less sensitive to changes as compared to paper with smaller pores. While one might think this observation to be caused by evaporation differences due to pore size, the authors found drift to vary minimally between paper substrates, disproving that hypothesis. An alternative explanation to account for the effect of pore size on the potentiometric response could not be provided [20].

Using paper-based sampling, several ions exhibited slopes larger than observed with analogous beaker-based setups [21,35]. When using crystalline solid-state ISEs,

responses increased by 3 mV/decade for Cl^- and by 6 mV/decade for Cd^{2+}, resulting in a super-Nernstian response, and Pb^{2+} exhibited a super-Nernstian response from 10^{-3}-10^{-4} M (see Fig. 5A). This super-Nernstian response was attributed to the binding of metal ions to the negatively charged hydroxyl groups of cellulose. At low concentrations, this effect was hypothesized to deplete the sample|ISM interface of target ions, explaining also that the shift to a super-Nernstian response at lower concentrations was so pronounced as to give a super-Nernstian jump [28].

Textile-based sampling has been shown to shift responses slopes towards both sub- and super-Nernstian responses. For Cl^- sensing with a crystalline solid-state sensor, there was no change in response slope from beaker to textile-based sensing. However, when using a conducting polymer containing solid-contact Cl^- ISE, response slopes were sub-Nernstian for all synthetic textiles but still Nernstian for cotton textiles [32]. In this case, the material-dependent shift in response slopes was attributed to the high redox sensitivity of the conducting polymers in the solid-contact electrode [32]. However, these same textiles exhibited Nernstian responses when used with solid-contact ISEs for Na^+ and K^+, indicating that the redox sensitivity of the PEDOT contact depends upon the target ion. When measuring Cd^{2+} and Pb^{2+} with crystalline solid-state ISEs, a shift from Nernstian to super-Nernstian slopes at lower concentrations was observed for all textiles, which was explained in terms of strengths of binding of the divalent cations to the cellulose or polyester blends used.

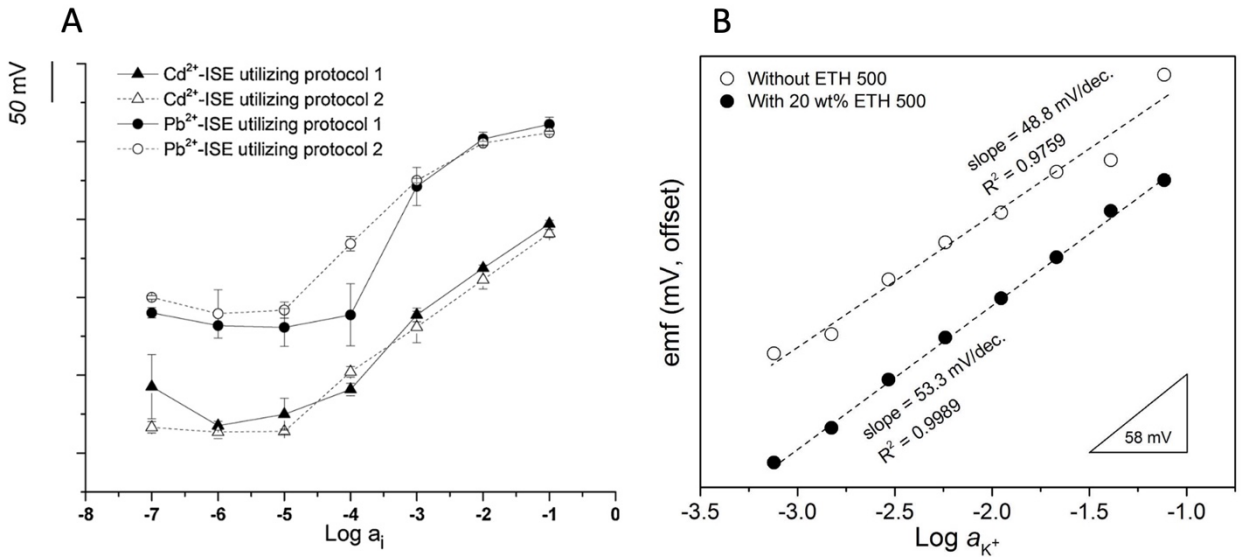

Figure 5. Potentiometric responses of Cd^{2+} and Pb^{2+} ISEs and filter paper-based sampling with pristine (Protocol 1) and inorganic salt-soaked filter paper (Protocol 2), (B) Potentiometric response of paper-based K^+ ISEs with and without tetradodecylammonium tetrakis(4-chlorophenyl)borate (ETH 500) in the ISM. Reproduced with permission from references, [28,58] respectively.

With solid-contact ISEs and a RE of a disposable 3 M KCl loaded paper in contact with a reusable Ag/AgCl element, Cl^- responses remained unchanged while K^+ responses increased by 3 mV/decade and Na^+ by 4 mV/decade [35].

The understanding of substrate–analyte interactions has led to successful elimination of non-ideal slopes. For example, in sponge-based sampling, adsorption of Cd^{2+} and Pb^{2+} by commercially produced polyurethane and cellulose sponges as well as natural sea sponges was quantified and used as a screening criterion to choose the ideal sponge for sampling. In this system, sponges were cut into $3 \times 2 \times 0.5$ cm^3 pieces and had macro-sized pores much larger than paper and textiles. Polyurethane sponges were

found to be ideal for Cd^{2+} and Pb^{2+} sensing due to their low sorption of those ions and were, therefore, used as the sampling material in subsequent potentiometric experiments. Nernstian responses were achieved for Cd^{2+} and Pb^{2+} as well as for K^+, Na^+, and Cl^- [30]. The physical structure of the material was not studied, and it would have been interesting to see potentiometric data for a cellulose-based sponge to confirm that response deviations were due to the chemical nature of materials rather than the pore structure.

Super-Nernstian responses in filter-paper based sampling were overcome by soaking paper in an inorganic salt of the target ion (see Fig. 4A) [28], pre-treating paper with various ISM components [29], or acidification with HCl.[31] Interestingly, when examining the effect of ISM-modified filter paper, the authors also found a super-Nernstian response when the ISM-modified filter paper was kept in contact with electrodes but placed into a beaker of sample solution, showing that in this case the sample volume does not affect performance [29].

Interferences depend upon chemical characteristics of the substrate as well as the identity of the target ion and can sometimes be overcome through modifications of the substrate.

4.4 Slopes in strip-type sensors

Nernstian responses were found for Na^+ and K^+ using substrate-based sampling with strip-type sensors comprising PET [25] (59.3 ± 0.3 and 59.1 ± 0.1 mV/decade for Na^+ and K^+, respectively) or paper coated with SWCNT/poly(3-octylthiophene) (58.4 ± 0.1 and 60.0 ± 0.4 mV/decade for Na^+ and K^+, respectively) [38]. In contrast to substrate-based sampling, here the underlying substrate was fully coated with SWCNTs, and there was no substrate/sample or substrate/ISM interface. However, slight sub-Nernstian responses

were found for Cd^{2+} (27.4 ± 0.4 mV/decade), Ag^{+} (54.2 ± 0.6 mV/decade), and K^{+} (56.7 ± 0.8 mV/decade) when filter paper was coated first with SWCNT, followed by Au and finally poly(3-octylthiophene) [37].

A super-Nernstian response (value not reported) was also found in the low concentration region (below 10^{-5} M) for strip-type sensors of CNT-coated filter paper coated with a K^{+} ISM. This was attributed to Na^{+} interfering ions introduced with the solid contact material, i.e., sodium carboxymethylcellulose contained in the CNT suspension used to prepare these sensors. It is interesting to note that the interference was observed in paper and not in conventional setups because of the different amounts of CNT suspension used [94]. Scaling considerations as this one are important to keep in mind; it was also shown that trace level contamination from conductive inks used for Cl^{-} sensing affects the performance with volumes of 20 µL sized samples but not 100 mL samples [95].

When using a strip-type sensor with ISMs drop-cast onto a 3D-drawn support of polylactide and carbon black composite, sub-Nernstian responses were observed for Ca^{2+} and Cl^{-}, but not K^{+} (for Ca^{2+}, Cl^{-}, and K^{+} 24.6 ± 1.2, -52.2 ± 0.3, and 55.5 ±0.6 mV/decade, respectively) [39]. In contrast to devices mentioned earlier in this section, where the underlying support was coated with CNTs, here the solid contact consisted of a thermoprocessable carbon black/polylactide composite drawn onto the underlying polylactide.

4.5 Slopes in sensors built on top of a substrate

K^{+} ISEs integrated with a RE were built on a PET substrate with conductive strips of carbon ink, a layer of SWCNT functionalized with octadecylamine groups, and either a

K^+ ISM or reference membrane. In these devices both membranes were made of a photo-cured poly(*n*-butylacrylate), and the K^+ ISM contained, in addition to standard ionophore and ionic site, 1 wt % ETH 500. Nernstian responses were observed both upon immersion in a beaker versus a conventional RE and with the integrated RE [40].

When using a screen-printed ISE with a plasticized, ionophore-doped ISM on graphene/PEDOT:PSS coated filter paper to measure in 20 µL sample droplets, Nernstian response slopes of 62.5 and 62.9 mV/decade were observed for Na^+ and K^+, respectively. Interestingly, the authors also noted that sub-Nernstian responses (43.6 and 46.1 mV/decade for Na^+ and K^+ respectively) were observed when graphene was not doped into the PEDOT:PSS, which they attribute to PEDOT:PSS's tendency to form a water layer [65].

An array of Na^+ and K^+ ISEs and a RE membrane drop-cast on Au screen-printed onto a polyimide substrate gave a sub-Nernstian response for Na^+ (43.76 mV/decade) but a Nernstian response for K^+ (57.38 mV/decade). Here, calibration conditions including the volume and composition of the sample solution are unclear as a pure salt solution and a phosphate buffer solution were used as samples for different experiments. Such information would help comparison with devices reported by other groups and the interpretation of the data, which was reported as concentrations instead of activities [82].

An array of ionophore-doped poly(vinyl) chloride (PVC) ISM/reduced graphene oxide/Au nanoparticle/carbon ink/Ag nanowire sensors for Ca^{2+}, AgCl/Ag ink for Cl^- detection and a RE, all on top of PDMS material, gave a Nernstian response for Ca^{2+} (28.53 mV/decade) but a sub-Nernstian response for Cl^- (-51.5 mV/decade). There are several possible factors that could explain the low slope, including ones already listed in

this review, i.e., use of concentrations instead of activities as well as possible interference from the sponge of an unspecified material used for sample uptake [60]. Lack of experimental details and control experiments make it difficult to come to a reliable conclusion.

Another sensor array included polystyrene nanospheres coated first with Au nanoparticles and then either Na^+ or K^+ ionophores and ionic sites, with the entire material referred to by the authors as “nanocomposite”. In addition, nanocomposites doped with Ag^+ ionophore were used for a calibration channel, which accounts for a signal background as urine, the chosen sample matrix, had a low concentration of Ag^+. When tested in simulated urine samples, the sensors gave sub-Nernstian responses to Na^+ (50.3 ± 1.3 mV/decade) and K^+ (53.5 ± 1.2 mV/decade).[45] As neither control experiments with the polystyrene-Au nanocomposites and a Ag^+ calibration channel, nor calibrations of the array in pure salt solution were reported, it is unclear whether the sub-Nernstian response was due to the ISE design, miniaturization, or interference from the urine matrix. In another system, proposed for epidermal sweat sensing, ISMs with a bis(2-ethylhexyl) sebacate (DOS) plasticized PVC matrix were drop cast on PET coated with screen-printed carbon [52]. Here a sub-Nernstian slope of 48.5 mV/decade was reported for Na^+ sensing. A poorly chosen selection of the range for the linear fit and the use of a Na^+ counter salt of the ionic site without equilibration of the ISM with K^+ solution (i.e., conditioning) prior to measurements may explain the low response slope. When a membrane that does not contain the primary ion (in this case, K^+) is exposed to a sample solution, the primary ion will transfer into the sensing membrane, exchanging with the counter ion of the ionic sites. Until this ion exchange is accomplished and the membrane

is saturated with water, potential drift is observed. Such initial potential drift can be minimized by using in the fabrication of the sensing membrane ionic sites paired with the primary ion [96]. Interestingly, the K^+ ISE gave a slightly super-Nernstian response of 63.1 mV/decade while the pH ISE had a response of 55.50 ± 6.31 mV/pH, which is within error Nernstian.

4.6 Slopes in Sandwich-Type Sensors

Sub-Nernstian responses have been observed in sandwich-type setups with filter paper with both ionophore-containing and ionophore-free sensing membranes. In ionophore-containing membranes, a sub-Nernstian slope of 22.9 ± 0.8 mV/decade was observed for Ca^{2+}, while closer to Nernstian responses of 54.9 ± 0.6 and 54.8 ± 1 mV/decade were observed for K^+ and Na^+, respectively [24]. In contrast, a membrane-free Cl^- sensing system with the same filter paper gave a Nernstian response (–61.8 ± 1.0 mV/decade). Another sandwich-type setup was developed for ionophore-free sensing of bilirubin (ISM of PVC, DOS, tridodecylmethylammonium chloride), which at a neutral pH is a divalent anion, and again a sub-Nernstian response (-22 mV/decade) was observed [56].

All the membranes mentioned in this section thus far have been PVC-based. However, the same sandwich-type setup was used with a 3D-printed ion exchange membrane composed of a photocured polyacrylate monomer, DOS as plasticizer, and tetrakis(*p*-chlorophenyl)borate as ion exchanger, and gave a response slope of 58.4 mV/decade [57].

4.7 Slopes for sensors with wicking capabilities and membranes incorporated into one a single unit

Sub-Nernstian slopes have also been reported in setups with membranes integrated into the underlying substrate. Using a hydrophilic high-capacity anion exchange membrane for Cl^- sensing and an ionic-liquid-based PVC reference membrane on a filter paper support, a Nernstian response was achieved with both an inner filling setup (-57.3 mV/decade) [58] and a redox-buffer doped colloid-imprinted mesoporous carbon solid-contact design (-60.6 mV/decade) [64]. When switching to an ionophore-doped PVC membrane for K^+ sensing, a sub-Nernstian response of 48.8 mV/decade was observed, but it was improved to 53.3 mV/decade by the addition into the ISM of 20 wt % ETH 500, an inert and very hydrophobic electrolyte salt (see Fig. 4B) [58]. While resistance may have played some role affecting this slope, it must be noted that ETH 500 decreased the resistance by less than an order of magnitude, and the 10.9 ± 1.2 MΩ initial resistance was significantly lower than the 10 TΩ input impedance of the potentiometer. At this time, the reason for the beneficial effect of ETH 500 is not clear.

A PET textile embedded with a PVC Cl^- ion exchange membrane with the same setup as the previous paper-based devices also gave a slightly sub-Nernstian response (55.5 ± 1.7 mV/decade). A hydrophilic high-capacity anion-exchange membrane was also incorporated into the polyester textile, but results were studied for serum samples only and not for aqueous KCl solutions, as for all the other work discussed here, so a comparison is difficult [59].

4.8 Slopes in textile-based sensors

In a cotton thread-based ISE with a graphite ink as solid contact and a conventional double-junction RE, slight sub-Nernstian responses were observed for Ca^{2+} (26.3 ± 0.5 mV/decade) and Cl^- (–52 mV/decade as estimated from a figure), while a Nernstian response was observed for K^+ (53.6 ± 0.7 mV/decade) and Na^+ (59.1 ± 1.1 mV/decade). The authors explored different support materials for K^+ sensing with the same graphite ink. Devices with a Nylon support exhibited slopes of 60.4 ± 4.0 mV/decade while those with a cotton support showed slopes of 55.2 ± 1.4 mV/decade but were not pursued due to poor standard electrochemical potential (E^0) reproducibility (± 26.8 mV, compared to ± 11.2 mV for the cotton thread-based devices). While the ISM was separated from the cotton thread by the graphite ink, it is clear that contact between the solid contact and support material may result in interactions between the graphite ink and thread [61].

Deviations in slope have also been reported for other textile-based setups with integrated REs. For CNT fibers coated with either an ISM or Ag/AgCl ink coated with a NaCl doped reference membrane, sub-Nernstian responses were observed for Na^+, K^+, and pH (45.8, 35.9, and 42 mV/decade, respectively, as estimated from a figure) while a large super-Nernstian response was observed for Ca^{2+} (52.3 mV/decade) [62]. The Na^+ salt of the ionic site was used for the preparation of each of these membranes, and membranes were not conditioned prior to measurements, which could explain the sub-Nernstian responses for K^+ and Na^+. It is also interesting to note that a single design here gives both super- and sub-Nernstian responses for different cations.

Overall, substrate-based sampling often results in increases in response slope compared to conventional sensing, while setups with the ISE and/or RE built into the

underlying material often result in sub-Nernstian responses, ultimately suggesting interactions between substrates and samples as the cause of these problems. A more complete understanding of the nature of possible interactions is made difficult to reach when the data analysis does not account for liquid junction potentials and activity coefficients or when a comparison to beaker-based measurements for analogous electrodes has not been performed.

5 Reproducibility

5.1 Overview of reproducibility in potentiometry

The term “calibration-free” has been used to refer to sensors with a low batch-to-batch standard deviation in the value of E^0 [14]. If E^0 is sufficiently reproducible from sensor to sensor, a single calibration curve may be performed on one sensor and used for all subsequent sensors. However, there is no universally acceptable value for the maximum acceptable SD of E^0 for such a purpose. Instead, the needs of each application dictate the tolerable errors. For example, for diagnostic tests, the U.S. Food and Drug Administration mandates a maximum acceptable error for Na^+ of ± 4 mM within the range of 80-200 mM, which translates to a 0.7 mV acceptable standard deviation for an ISE [97], while manufacturers of clinical mainframe analyzers, which are recalibrated very frequently, strive for substantially narrower confidence intervals.

Unfortunately, reproducibilities are often not reported for miniaturized sensors. A range of parameters, such as % RSD of several electrodes of the same batch [71,74,98], day-to-day reproducibility of the same sensor [99], SD of the EMF at a single concentration [43,56], averages of the SDs for various electrodes in the same solution

within the linear range [23,25], confidence intervals calculated from student's t-tests [83], and vague statements on SD [39,57,66,77], have been reported, which makes direct comparisons often difficult. Relative errors of E^0 are not a helpful parameter to report, as E^0 values vary by orders of magnitude and, therefore, are not comparable across devices. Some literature reports include the % RSD as well as the average E^0, in which case the reader can calculate the SD of E^0; however, this appears unnecessarily complicated. Therefore, we discuss in the following only articles that reported the SD of E^0 (or % RSD along with an average E^0).

5.2 Reproducibility of E^0 in miniaturized ISEs

The reproducibility of E^0 of miniaturized ISEs as prepared in research laboratories is generally on the order of several mV and is often attributed to their handmade nature. An early report of a rectangle (presumably of standard toner ink) laser-printed on PET, coated first with a PEDOT:PSS solid contact and then a Ca^{2+} ISM, gave a SD of E^0 of 0.7 mV [36]. In thread-based sensing, a cotton thread painted with conductive ink and dip-coated in ISMs gave E^0 SDs of 2.3, 3.4, 2.6, and 0.5 mV "or better" for K^+, Na^+, Ca^{2+}, and Cl^-, respectively [61]. However, both types of sensors were used with non-miniaturized double-junction REs and beaker-based sampling.

Steps towards integrated devices include a RE in an array of sensors built up on top of a substrate. For an array made of graphene paper strips dipped into a tetrahydrofuran solution of *o*-NPOE as plasticizer, PVC, ionophore, and ionic sites, and laid on a piece of plastic for solvent evaporation, with no underlying support for the solid contact, E^0 SDs of 18, 21, and 16 mV were reported for K^+, Ca^{2+}, and pH, respectively. It is unclear whether this data was obtained with a miniaturized RE comprising a photocured

polyacrylate reference membrane doped with KCl, AgCl, and ETH 500, or whether a non-miniaturized double-junction RE was used. The high SDs were hypothesized to be due to inhomogeneities in the thickness and composition of the graphene paper and poor adherence between paper and the ISM [100].

Another array, with polystyrene nanospheres coated first with Au and then with ionophores and ionic sites for Na^+ and K^+ sensing, polystyrene nanospheres surface-functionalized with Au for a Ag^+ ISE-based calibration channel, and a NaCl doped poly(vinyl butyral) RE had an E^0 SD of 5.6 and 6.0 mV (n=10) for Na^+ and K^+, respectively [45]. Unfortunately, in both of these arrays, the experimental details do not clearly state whether the arrays were used by dipping into beakers that contained the sample solutions or by dropping samples onto them, and whether data was from use of a custom RE or a non-miniaturized RE. Such details are important to assess the effects of miniaturization on the device performance.

Integrated sensors that use a wicking material allow for the use of a sample size close to clinical relevance (20-30 µL). Textile-based devices with an embedded ISM and an ionic-liquid-based reference membrane showed similar SDs for PVC-based Cl^- ion exchange membranes used to measure in aqueous and serum samples (4.2 and 3.5 mV, respectively) and for hydrophilic high-capacity anion-exchange membrane used to measure in serum (3.0 mV) [59]. Paper-based devices with the same type of reference membrane showed similar reproducibilities with a hydrophilic high-capacity chloride-exchange membrane in aqueous samples and serum, as well as with K^+ ionophore containing ISMs (SD of 2.0, 1.6, and 1.6 mV) [58]. For comparison, paper infiltrated with the hydrophilic high-capacity anion-exchange membrane was also tested in a

conventional setup and gave a SD of 2.2 mV, showing that the sensor miniaturization did not worsen the reproducibility. In another similar setup, fully-inkjet-printed sensors with a lipophilic salt containing reference membrane and ionophore containing ISMs gave a SD of 5.1 and 2.8 mV for Na^+ and K^+ sensing, respectively.

Some articles compare the performance of miniature ISEs when used with conventional and miniaturized REs, which allows analysis of the effect of miniaturization of the RE on reproducibility. Lithium ion sensing yarns gave a SD of 8.7 mV when tested against a double junction RE but 13.0 mV when tested against a Ag/AgCl-coated carbon fiber dip-coated with a reference membrane [71]. An ion patch for $Cl^–$, K^+, Na^+ and pH detection was tested with respect to both a double-junction RE and a patch RE. While the SD of E^0 as measured with a non-miniaturized RE and a patch RE showed minimal differences for $Cl^–$ sensing (5.2 to 6.8 mV, respectively), it decreased significantly for Na^+ sensing (from 12.7 to 0.3 mV), and increased for pH sensing (4.6 to 12.5 mV), suggesting analyte specific effects of RE integration [68].

5.3 Reproducibility of E^0 in sensors specifically designed for high reproducibility

Some of the recent work on miniaturized sensors has specifically focused on improving the E^0 reproducibility. One strategy is based on the use of a molecular redox buffer that resists changes in the phase boundary potential at the interface between the ISM and the underlying electron conductor, much like a pH buffer resists changes in the pH of a solution. In the first example for incorporation of equimolar amounts of redox buffers into miniaturized sensors, the hydrophobic redox buffer cobalt(II/III)tris(4,4′-dinonyl-2,2′- bipyridyl) was included into both the ISM and an ionic-liquid-based reference membrane, both overlying a colloid-imprinted mesoporous carbon solid contact [63]. In

this fully-integrated paper-based device, a SD of 2.1 mV was obtained, compared to a SD of 2.8 for an analogous conventional setup.

In another attempt to use a hydrophobic redox buffer, the prior design was modified by incorporating into the sensing membrane the redox buffer comprising 7,7,8,8-tetracyanoquinodimethane and the corresponding anion radical [64]. While use of this redox buffer in a conventional setup resulted in a fairly small SD of 4.3 mV without conditioning, after 24 h, the SD increased to 14.0 mV. Translation to a paper-based setup resulted in poor linearity, and the SD of E^0 was not reported. There is clearly a need for more hydrophobic redox buffers that do not leach out of the ISM.

In addition to hydrophobic redox buffers, a hydrophilic redox buffer, consisting of cobalt(II/III) bis(terpyridine), was also proposed for use in anion-sensing polymeric sensing membranes. The complex was added into the inner filling solution of conventional, rod-shaped chloride sensors, decreasing the SD from 2.7 to 0.3 mV as compared to conventional rod-shaped electrodes with an inner filling solution of 1 mM KCl. Textile-based devices with embedded membranes and a Au wire as electron conductor were fabricated with the same redox buffer in the inner filling solution and resulted in a SD of E^0 of 3.8 mV, a significant improvement over previous devices with a similar design [101].

It has also been proposed that redox-active species do not have to form a redox buffer to stabilize E^0. Specifically, CNT-coated filter paper was coated with a CNT layer doped with both a cobalt(II)porphyrin and cobalt(III)corrole before drop casting of a K^+ ISM. Indeed, a low SD of 1.7 mV was obtained on Day 1 and found to be even lower (0.6 mV) on Day 2. It was suggested that the high reproducibility and stability over time

resulted from the ability of the porphyrinoids to limit ion-fluxes across the sensing membrane [94]. However, it has also been shown that in such a system even small impurities in redox active reagents result in redox pairs, which then control the interfacial potentials, thereby negating the argument that non-paired redox couples improve E^0 reproducibility [102].

In other work, ferrocyanide and ferricyanide in a ratio of 6.9:1 were used as redox buffer species in the transduction layer of miniaturized ISEs to improve the E^0 reproducibility. Screen-printed electrodes with a potassium ferrocyanide doped carbon layer and a drop cast K^+ ISM exhibited an E^0 SD of 2.8 mV during 24 to 36 h of conditioning (see Figs. 6A and B). The authors suggested the use of equimolar amounts of ferrocyanide:ferricyanide in future work to further improve reproducibilities [103].

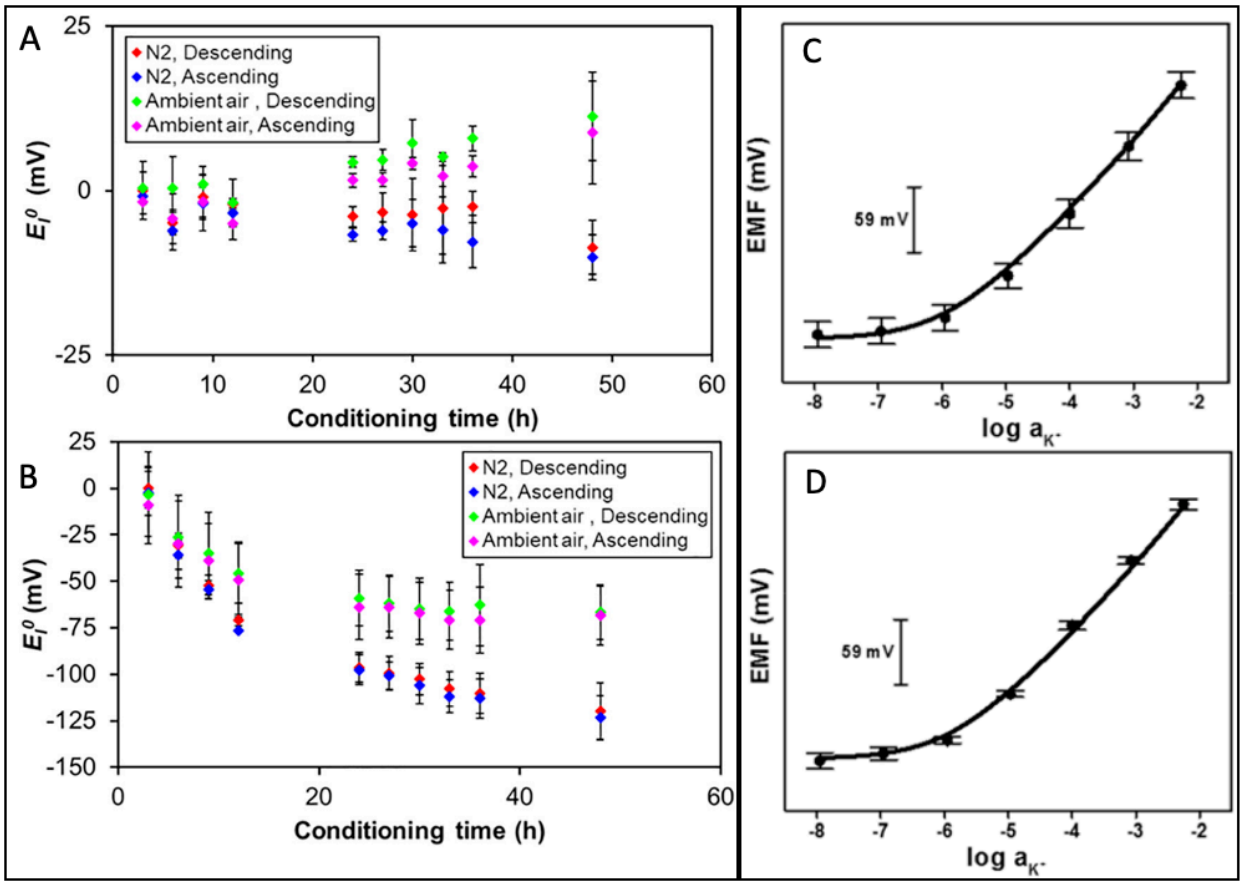

Figure 6. E^0 for screen-printed ISEs in various conditioning environments (A) with and (B) without ferrocyanide in the solid-contact layer. Potentiometric response of strip-type ISEs with (C) tetrahydrofuran and (D) cyclohexanone as the solvent in the ISM. Reproduced with permission from references [36,99], respectively.

The reproducibility of strip-type ISEs with supporting substrates coated with SWCNTs, poly(3-octylthiophene), and PVC-based ISMs has been optimized by systematic variation of the fabrication procedure [38]. The SD of the EMF of 3 devices immersed into the same solution, rather than the SD of E^0 was provided, but one may assume that these values are similar. The use of cyclohexanone rather than

tetrahydrofuran as the solvent for the ISM components was found to improve the SD of the EMF for K^+ ISEs as measured in 10^{-5} to 10^{-2} M KCl samples from approximately 10 mV to 5.0 mV, due to the solvent-dependent dissolution of poly(3-octylthiophene) upon drop casting of the ISM (see Figs. 6C and D). Additionally, single-step integration of a poly(3-octylthiophene)/SWCNT solution rather than a 2-step deposition further improved the E^0 SD to 2.0 mV for K^+ ISEs, attributed to increased hydrophobicity. These are significant improvements compared to earlier work with CNT-coated paper strip sensors with reported SDs of "as much as 30 mV" [23] and 10 mV [37]. Applying these two improvements to the fabrication of ISEs, arrays of PET-based sensor strips gave an E^0 SD of 1 mV or less for Na^+ and K^+ in both aqueous and artificial sweat samples, showing that the SD does not worsen in a complex matrix [23,25].

Short-circuiting multiple electrodes to a RE is another recent strategy shown to improve reproducibilities in the E^0 of conventional solid-contact K^+ ISEs [104]. This method was also used with carbon-fiber based Na^+ ISEs, improving the E^0 SD at the time of the first measurement from 37.6 to 1.45 mV (n=4) for sampling in aqueous solution against a conventional double-junction RE [74]. While a carbon-fiber based RE was also developed and used for testing in an integrated setup with artificial sweat, repeatability was reported only for the response slope. Visual inspection of the calibration plot suggests a worsened SD of E^0 [74]. While there are some interesting and promising approaches to improve the reproducibility of E^0, more standardized reporting will enable better comparison of performance across sensor designs.

6 Lower limits of detection (LOD)

6.1 Lower LODs in ion-selective potentiometry

By well-accepted convention, the lower LODs of ISEs are determined by extrapolation of the linear EMF response to the value observed when no target ion is added to the sample [105]. Therefore, when dynamic ranges are mentioned in this section, it is because no LOD was reported. As the failure to account for activity coefficients or liquid junction potentials impacts LOD calculations only marginally, these effects are not mentioned in this section.

6.2 Common sources of worsened lower LODs

In reviewing the relevant literature, we noticed two common sources of worsened LODs for miniaturized ISEs, that is, interactions between analytes in samples and underlying substrates as well as contamination from sensor materials.

Interactions of target ions with components of the sensor device other than the ISM may result in alterations to the concentration of the target ion in the sample and, thereby, increases in the lower LOD. Adsorption of heavy metals onto the negatively charged cellulose chains of paper was shown to cause poor LODs in paper-based sampling systems [30]. A lack of response to heavy metal ions at low sample concentrations followed by a super-Nernstian response upon gradually increasing the sample concentration distorts the calibration curve, reducing the range of the Nernstian response (Figure 5A) [21,28,31]. These responses look very similar to those observed for non-miniaturized ISEs at very low concentrations when ion fluxes across the ISM occur [93], but they may result from a combination of the adsorption of heavy metal ions to the device substrate and transmembrane ion fluxes.

Contamination of samples by components of the sensing device has also been shown to explain worsened lower LODs in some paper-based devices. In small-volume potentiometric devices, even ppm level contaminants that leach off solid-contact materials, such as conductive inks or supporting substrates, can increase analyte concentrations and worsen the LOD [94,95]. Observing an improvement in textile-based devices compared to analogous paper-based ones, especially in membrane-free systems, a systematic study of the effect of materials on lower LOD was performed. It was found that both the filter paper and the Ag/AgCl ink used as transducer leached small amounts of Cl^- ions, which, due to the small sample volumes, significantly biased the Cl^- concentration in samples (Figure 7) [95].

A

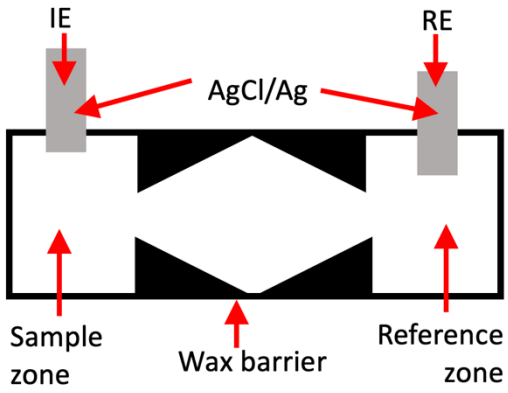

B

AgCl/Ag Form	Setup	LOD (M)
Ink	Paper-based	$10^{-3.4 \pm 0.3}$
Ink	Textile-based	$10^{-4.1 \pm 0.1}$
Ink	Au electrodes in beaker	$10^{-4.8 \pm 0.1}$
Ink*	Au electrodes in beaker*	$10^{-5.0 \pm 0.1}$
Wire	Paper-based	$10^{-4.0 \pm 0.2}$
Wire	Textile-based	$10^{-4.4 \pm 0.1}$
Wire	Beaker	$10^{-4.9 \pm 0.1}$
Wire	Beaker*	$10^{-4.8 \pm 0.1}$
Plate	Paper-based	$10^{-3.9 \pm 0.1}$
Plate	Beaker	$10^{-4.8 \pm 0.1}$

Figure 7. (A) Schematic of substrate-based devices used and (B) table of potentiometric characteristics for Cl^- of devices with different types of AgCl/Ag transducers and substrates (*data corresponds to Ag^+ sensing). Adapted with permission from reference [95].

6.3 Lower LODs of sensors with substrate-based sampling

When coupling conventional solid-contact ISEs with substrate-based sampling, the lower LOD is generally worsened by an order of magnitude or larger as compared to conventional measurements in beakers. Early work using nitrocellulose paper for sampling with a Ag^+ ISE as indicator and Ca^{2+} ISE as pseudo RE resulted in an LOD of 10^{-5} M, as compared to 10^{-8} M for beaker-based sampling. The significant worsening of the lower LOD was posited to be due to either sluggish mass transport of Ag^+ or adsorption of Ag^+ onto cellulose [19]. However, using atomic emission spectroscopy, it has been shown more recently that adsorption of Ag^+ to paper occurs only at high concentrations [95]. In light of this finding, one may wonder whether sluggish mass transport of Ag^+ was responsible for the poor lower LOD in the work with nitrocellulose paper.

Filter paper sampling with a solid-contact K^+-ISE and solid-contact RE also resulted in worsening of the LOD for K^+ sensing by 3 orders of magnitude, with the exact value depending on the shape of the paper sampling unit [20], and a slightly less than one order of magnitude worsening for Na^+ sensing [27]. However, when using a single-junction RE with paper sampling, the lower LOD of a solid-contact Cl^--ISE was the same ($10^{-5.0}$ M) in both paper and beaker-based sampling [21]. Interestingly, when replacing the RE with a paper-based reference unit coupled to a reusable AgCl/Ag rod, the LOD for a solid-contact Cl^- ISE increased to $10^{-4.1 \pm 0.1}$ M, indicating that interactions of both sensing and reference electrodes with supporting substrates can affect the lower LOD [35]. This worsened LOD was consistent across all ions sampled; Na^+ and K^+ gave LODs of $10^{-4.1 \pm 0.1}$ and $10^{-3.3 \pm 0.1}$ M, respectively [35].

A number of approaches have been tested to alleviate this problem. The largest improvement of the lower LOD for Pb^{2+} sensing (to $10^{-5.4}$ M) was achieved by soaking a 2 cm x 2 cm piece of filter paper in an ISM solution (PVC, *o*-NPOE, potassium tetrakis(4-chlorophenyl)borate, tert-butylcalix[4]arene-tetrakis(*N,N*-dimethylthioacetamide), THF) for 30 min, and allowing the solvent to evaporate overnight. Elemental mapping of paper revealed ISM components concentrated along the cellulose fibers rather than filling pores between fibers and penetration through the paper, as can be seen in cross-sectional images (see Figure 8). This pretreated paper was then used for paper-based sampling with a rod-shaped solid-contact Pb^{2+} ISE. It was hypothesized that coating the paper with the ISM altered the physiochemical state of the filter paper that was in contact with the conventional ISE, improving the sensor performance. The LOD did not change when modified sampling paper was held in contact with the solid-contact ISE and submerged in a beaker of sample, indicating that the worsening of the LOD does not depend on the volume of the sample solution [29].

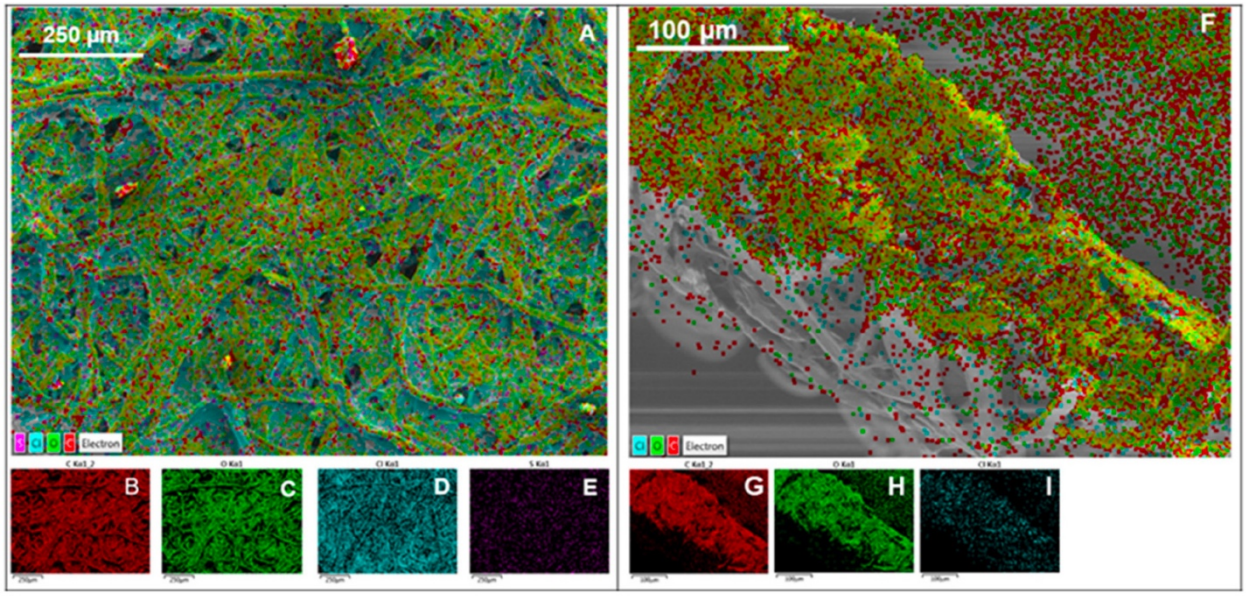

Figure 8. Elemental mapping of the surface (left) and cross-section (right) of ISM-modified paper, where Panels A and F show the overlapped elemental images, and B to E as well as G to I show the individual element maps of carbon (red), oxygen (green), chlorine (light blue), and sulfur (purple). Reproduced with permission from reference [29].

Lower LODs were also worsened in sampling with non-paper substrates. In textile-based sampling, a deterioration of the LOD by 0.1 to 1.0 orders of magnitude was observed for the detection of Cd^{2+}, Cl^{-}, and Na^{+}, the LOD worsening depending on the composition of the textile (cotton, polyester, polyamide, and blends with elastane). Interestingly, there was only a minimal worsening of the LOD for K^{+} sensing [27,32]. Similarly, for polyurethane sponge-based sampling, Cl^{-} and Pb^{2+} sensing was affected by substantial worsening of the LOD, while LODs for K^{+}, Na^{+}, and Cd^{2+} were hardly affected. While heavy metal adsorption was examined experimentally and explained the difference in effects observed for Pb^{2+} and Cd^{2+}, the reason for the worsening in Cl^{-} sensing is yet unexplained [30].

6.4 Lower LODs in strip-type sensors

Strip-type sensors, in which only the transducer is in contact with the substrate, are tested in large volume samples and generally exhibit LODs similar to, or within one order of magnitude of, those of analogous conventional ISEs.

For early strip sensors with electropolymerized PEDOT/PSS solid contacts on a PET substrate, lower LODs of $10^{-8.3}$ and $10^{-6.4}$ M were achieved for Ca^{2+} and K^{+} sensing through optimization of the ratio of PEDOT and PSS and the membrane thickness [36]. Strip-type ISEs with a carbon solid contact coupled with a conventional RE also result in LOD values that were within an order of magnitude of those for analogous non-miniaturized ISEs for Cu^{2+}[48], the antidiabetic ionic drug pioglitazone,[22] as well as K^{+}, Ca^{2+} and Cl^{-}[39]. Interestingly, solid-contact ISEs based on filter paper coated with carbon ink exhibited a half an order of magnitude worsened LOD for Ca^{2+} sensing, but a two orders of magnitude worsened LOD for Mg^{2+}. These 2 strips were then incorporated into an array with an integrated RE, but LODs were not reported for this modified setup [26].

SWCNT-coated filter paper used as a supporting substrate resulted in LODs in the micromolar range for K^{+} and NH_4^{+} [23]. However, in subsequent work, the same design of paper-based ISE with a Li^{+} ISM resulted in a half an order of magnitude worsened LOD as compared to conventional ISEs, showing again the effect of miniaturization being dependent upon the target ion identity. When testing artificial serum, coupling the paper-based Li^{+} ISE with a paper-based RE did not affect the LOD significantly ($10^{-4.1}$ M) [43].

Work has also been performed to improve the lower LOD of strip-type sensors to the nanomolar range through adaptation of fabrication techniques first introduced in conventional electrodes. By coating SWCNT-coated filter paper with Au and then a

poly(methyl methacrylate-*co*-decyl-methacrylate) based ISM, nanomolar detection limits were achieved for Cd^{2+}, Ag^{+}, and K^{+} [37]. Additionally, LODs on the order of 10^{-7} M for both K^{+} and I^{-} sensing were achieved with SWCNT-coated filter paper, sputter-coated with Au and then overlaid first with a poly(3-octylthiophene) solid contact and then with PVC-based ISMs. Replacement of the conventional RE using a paper-based RE with an ionic-liquid-based poly(methyl methacrylate-*co*-decyl methacrylate) reference membrane resulted in an order of magnitude worsening for Na^{+} but a minimal change for I^{-} [44]. While these methods do achieve very low LODs, they require Au sputtering, which complicates fabrication.

6.5 Lower LODs of sensors built on top of the substrate

A K^{+} ISE integrated with a RE was built on a PET substrate with conductive strips of carbon ink, a layer of SWCNT functionalized with octadecylamine groups, and either a K^{+} ISM or reference membrane. In these devices, both the ISM and reference membrane were made of a photo-cured poly(*n*-butyl acrylate), and the K^{+} ISM contained, in addition to ionophore and ionic sites, 1 wt % ETH 500. Lower detection limits comparable to those for conventional solid-contact K^{+} ISEs were found with both a conventional RE ($10^{-6.6}$ M) and the integrated solid-contact RE ($10^{-6.5}$ M), indicating that this type of RE does not significantly affect the responses in the lower concentration range [40].

For a sensor array made of initially free-standing graphene paper strips dipped into solutions of the ISM components and then placed side by side onto a plastic, there was minimal difference in the LODs between conventional and miniaturized sensors for K^{+}, Ca^{2+}, and pH sensors, although the reported work does not clarify whether the data that was reported is from testing with a conventional or a paper-based graphene RE [100]. An

array of 4 sensors prepared by Ag screen-printing on synthetic polypropylene paper and ISMs of polystyrene nanospheres coated first with Au and then with ISM gave for artificial urine LODs of $10^{-4.2}$ and $10^{-4.3}$ M for Na^+ and K^+, respectively [45]. As there no data on the use of these nanocomposite-containing ISM components in conventional electrode bodies was reported for comparison, these LODs are difficult to assess.

Another array built on a PDMS supporting substrate with a NaCl-doped poly(vinyl butyral) RE and C/Au/reduced graphene oxide/ISM for Ca^{2+} sensing gave a slightly worse LOD than in conventional setups. In the same array, a Ag/AgCl ink based Cl^- ISE resulted in an LOD of $10^{-3.3}$ M, significantly higher than the $10^{—4.8}$ M that is expected based on the solubility of AgCl [60]. While the authors did not attempt to explain the LOD, it may be due to Cl^- leaching from either the RE or the Ag/AgCl ink [95].

When using a polyurethane substrate with screen-printed carbon and AgCl/Ag ink, an order of magnitude worsening of the lower end of the linear range was found for Cl^-, Na^+, and K^+ but not for pH sensors (LOD not reported) as compared to corresponding values for analogous non-miniaturized ISEs. As the pH measurements were performed using pH buffers, it is possible that the pH buffers' ability to maintain a constant pH may have prevented pH changes in the sample but depletion of the other ions caused the poor LOD observed for the non-buffered solutions of the other ions. This array included a RE with an ionic-liquid-based reference membrane. This worsening may be due to the miniaturization of either the working or sensing electrodes [68].

An epidermal sensor with a PET support, screen-printed carbon ink as the solid contact, and drop cast ISMs resulted in a 1 mM LOD for both Na^+ and K^+ sensing [52]. While these values are more likely the lower end of the dynamic range rather than an

LOD calculated from extrapolation of values below the lower limit, it is still a significant deviation from the range of conventional electrodes of similar membrane compositions.

A comparison of the performances of the solid contacts for a Cd^{2+} ISE built on top of a PET substrate revealed that graphene resulted in an order of magnitude improvement in the lower LOD compared to graphite [47].

For all these devices with minimal contact between substrate and either the sample solution or ISMs, the extent of LOD worsening depends on the valency and identity of the measured ion as well as the type of solid contact used. Of 15 publications that report sensors built on top of a support substrate [25,26,40,43–49,51,52,60,68,100], six exhibited a lower LOD worsened at least half an order of magnitude upon miniaturization [43,45,49,52,60,68], seven showed a smaller or no deterioration of the lower LOD [26,40,44,46–48,100], and two did not report lower LODs or did not describe how the LOD was determined [25,51].

6.6 Lower LODs of sensors with higher levels of device integration

Integrated single-use setups with both the sample and sensing components in direct contact with the supporting substrate generally have a lower LOD that is more than one order of magnitude worse than for analogous conventional ISEs. A paper-based sandwich-type ISE exhibited a one order of magnitude worsening of the dynamic range for Na^+, K^+, and Ca^{2+} sensing [24] and a three orders of magnitude worsening of the LOD for ionophore-free bilirubin sensing [56]. In contrast, for a paper-based sandwich-type ISE with a 3D printed ion sensing membrane, there was no change in the dynamic range for ionophore-free tetrabutylammonium sensing [57].

Similarly high LODs have also been reported for devices with membranes embedded within the substrate material. A fully inkjet-printed paper-based device with PVC ISMs resulted in LODs of $10^{-4.0}$ and $10^{-4.5}$ M for K^+ and Na^+, respectively [65]. While no direct comparison was given for analogous conventional ISEs, these values are at least one order of magnitude worse than was reported elsewhere for conventional rod-shaped ISEs with the same ionophores [106]. Additionally, a paper-based device with an ionic-liquid-based reference membrane and K^+ ISM exhibited an LOD of $10^{-3.1}$ M K^+ [58], higher than for a non-miniaturized ISE of the same ionophore (valinomycin). The same setup with a hydrophilic high-capacity ion exchange membrane for Cl^- sensing gave a lower range of 10^{-3} M, similar to that of conventional devices [59].

In another device designed as a wearable sensor, hydrophobic barriers of poly(acrylonitrile-*co*-butadiene-*co*-styrene) films were transferred onto a cotton shirt, and the LOD for the Ca^{2+} ISE was reported as $10^{-5.2}$ M. However, it is unclear how the LOD was determined and whether the electrodes and membranes were printed directly onto the cotton material or built up vertically, as in other sensors for sweat, both factors that prevent direct comparisons between designs [66].

6.7 Lower LOD of textile-based sensors

A commercial carbon fiber coated with a Na^+ ISM and tested with a conventional RE resulted in an LOD of $10^{-6.3}$ M, similar to a conventional ISE. However, switching to a fiber-based RE with a NaCl doped poly(vinyl butyral) membrane, a cotton pad for wicking of samples, and artificial sweat, the lower limit increased to about $10^{-3.5}$ M, as estimated from a calibration curve. Unfortunately, it is difficult to pinpoint the cause of the poor LOD as many variables were changed at once [74].

An integrated device with SWCNT-coated cotton fibers dip-coated as a pretreatment in either a Li^+ ISM or a reference membrane solution resulted in an LOD of 10^{-5} M [71], which is similar to that reported for paper-strip type Li^+ ISEs of similar composition [43] but once again higher than for a conventional solid-contact Li^+ ISE. The similarity of the LODs for these 2 setups suggests that there was no effect of the identity of the substrate on the LOD, perhaps because the substrates are not in contact with the selective sensing components or sample. Additionally, for sensors with the same SWCNT and ISM composition, switching from filter paper to cotton yarn as the underlying substrate minimally affected the LODs, which were found for K^+, NH_4^+, and pH at $10^{-5.1}$ M, $10^{-5.4}$ M, and pH 10 for the paper substrate and 10^{-5} M, 10^{-6} M, and pH 11 for the yarn, respectively [23,83].

7 Conclusions

Overall, deviations from theoretically predicted device characteristics and performances of analogous non-miniaturized devices have been observed more often in miniaturized devices when there is direct contact between unmodified supporting substrates and sample solutions or sensing/reference membranes. When such contact is present, deviations often depend upon the chemical structure of the underlying support. Many modifications of supporting substrates have been shown to eliminate or lessen such effects. However, such modifications increase the complexity of the fabrication process and device costs to some extent and, therefore, need to be evaluated in the overall context of the required traits of a point-of-care device. On the other hand, fewer deviations from ideal sensor performance have been observed when the surface of the substrate

supporting the device is covered either by a solid-contact material or hydrophobic coating, completely separating the sample as well as the sensing and reference membranes from the substrate. In these situations, LODs do not correlate to the substrate structure and are typically found to depend primarily on the identity of the solid contact as well as the valency and identity of the measured ion. While there are many applications for which very low LODs are not required, non-theoretical response slopes cast doubts on the reliability of any device that exhibits them, and a high reproducibility of E^0 is critical for any sensor used in a calibration-free mode.

The incorporation of nanomaterials into many sensors reviewed in this paper demonstrates the nuances of selecting appropriate materials. Nanomaterials have to date primarily served as solid contacts, such as the CNTs on paper or threads [23,40,61]. However, nanoparticle-based conductive inks or wires have also been used to connect the solid-contact material to external wires [62,75]. As also observed for conventional ISEs, the use of nanomaterials as solid contacts may lead to improved reproducibility or even lower LODs [25,37]. Additionally, by fully coating the underlying support with a nanomaterial, there is no sample|substrate or sample|ISM interface, thereby preventing interactions that may lead to non-ideal performance. However, as with all materials in contact with small sample volumes, there is a higher risk of contamination of the sample by nanomaterials [94,95], and the impact of nanomaterials on cost, manufacturability, and ultimate disposal must be considered as well.

The systematic study of interactions between supporting materials. on one hand, and target analytes and components of reference electrodes, on the other hand, has increased our understanding of the source of non-ideal performances. Thereby, it has

also led to modifications that improve the sensor performance. Although the quantification of these interactions is complicated by the small sample volumes used in miniaturized devices, creative applications of fundamental analytical chemistry techniques will facilitate proper study. Continued study of the effects of miniaturization will hopefully lead to performances that meet the needs of point-of-care devices.

Declaration of competing interest

The authors declare that they have no known competing financial interests or personal relationships that could have appeared to influence the work reported in this paper.

Acknowledgments

This work was supported by the National Science Foundation (CHE-1710024, CHE-2203752) to P.B., and a Graduate Research Fellowship from the National Science Foundation and a 4th year excellence fellowship from the Department of Chemistry, University of Minnesota, to E.J.H.

8 References

[1] A. Lewenstam, Routines and Challenges in Clinical Application of Electrochemical Ion-Sensors, Electroanalysis 26 (2014) 1171–1181. https://doi.org/10.1002/elan.201400061.

[2] M. Borchardt, C. Diekmann, C. Dumschat, K. Cammann, M. Knoll, Disposable Sodium Electrodes, Talanta 41 (1994) 1025–1028. https://doi.org/10.1016/0039-9140(94)E0107-3.

[3] C. Diekmann, C. Dumschat, K. Cammann, M. Knoll, Disposable reference electrode, Sens. Actuators B Chem. 24–25 (1995) 276–278. https://doi.org/10.1039/a708992i.

[4] S. Walsh, D. Diamond, J. McLaughlin, E. McAdams, D. Woolfson, D. Jones, M. Bonner, Solid-State Sodium-Selective Sensors Based on Screen-Printed Ag/AgCl Reference Electrodes, Electroanalysis 9 (1997) 1318–1324. https://doi.org/10.1002/ELAN.1140091704.

[5] P.B. Deroco, D. Wachholz Junior, L.T. Kubota, Paper-based Wearable Electrochemical Sensors: a New Generation of Analytical Devices, Electroanalysis 2200177 (2022) 1–11. https://doi.org/10.1002/elan.202200177.

[6] M. Parrilla, M. Cuartero, G.A. Crespo, Wearable potentiometric ion sensors, Trends Anal. Chem. 110 (2019) 303–320. https://doi.org/10.1016/j.trac.2018.11.024.

[7] V. Krikstolaityte, R. Ding, E.C. Hui Xia, G. Lisak, Paper as sampling substrates and all-integrating platforms in potentiometric ion determination, Trends Anal. Chem. 133 (2020) 116070. https://doi.org/10.1016/j.trac.2020.116070.

[8] A. Sinha, Dhanjai, A.K. Stavrakis, G.M. Stojanović, Textile-based electrochemical sensors and their applications, Talanta 244 (2022) 123425. https://doi.org/10.1016/J.TALANTA.2022.123425.

[9] H. Curme, R.N. Rand, Early history of Eastman Kodak Ektachem slides and instrumentation, Clin. Chem. 43 (1997) 1647–1652.

[10] R.E. Calem, Moving the Common Blood Test Closer to the Patient, N. Y. Times (1992) 12.

[11] D. Mabey, R.W. Peeling, A. Ustianowski, M.D. Perkins, Diagnostics for the developing world, Nat. Rev. Microbiol. 2 (2004) 231–240. https://doi.org/10.1038/nrmicro841.

[12] N.P. Pai, C. Vadnais, C. Denkinger, N. Engel, M. Pai, Point-of-Care Testing for Infectious Diseases: Diversity, Complexity, and Barriers in Low-And Middle-Income Countries, PLoS Med. 9 (2012). https://doi.org/10.1371/journal.pmed.1001306.

[13] Y. ElSaboni, J.A. Hunt, J. Stanley, C. Moffatt, Y. Wei, Development of a textile based protein sensor for monitoring the healing progress of a wound, Sci. Rep. 12 (2022). https://doi.org/10.1038/s41598-022-11982-3.

[14] C.R. Rousseau, P. Bühlmann, Calibration-free potentiometric sensing with solid-contact ion-selective electrodes, Trends Anal. Chem. 140 (2021). https://doi.org/10.1016/j.trac.2021.116277.

[15] E. Bakker, Can Calibration-Free Sensors Be Realized?, ACS Sens. 1 (2016) 838–841. https://doi.org/10.1021/acssensors.6b00247.

[16] A.A. Kumar, J.W. Hennek, B.S. Smith, S. Kumar, P. Beattie, S. Jain, J.P. Rolland, T.P. Stossel, C. Chunda-liyoka, G.M. Whitesides, From the Bench to the Field in Low-Cost Diagnostics : Two Case Studies, Angew. Chem. Int. Ed. 54 (2015) 5836–5853. https://doi.org/10.1002/anie.201411741.
[17] W. Mazurkiewicz, M. Podrażka, E. Jarosińska, K. Kappalakandy Valapil, M. Wiloch, M. Jönsson-Niedziółka, E.K. Witkowska Nery, Paper-based electrochemical sensors and how to make them (work), ChemElectroChem 7 (2020) 2939–2956. https://doi.org/10.1002/celc.202000512.
[18] J. Mettakoonpitak, K. Boehle, S. Nantaphol, P. Teengam, J.A. Adkins, M. Srisa-Art, C.S. Henry, Electrochemistry on Paper-based Analytical Devices: A Review, Electroanalysis 28 (2016) 1420–1436. https://doi.org/10.1002/elan.201501143.
[19] J. Szűcs, R.E. Gyurcsányi, Towards Protein Assays on Paper Platforms with Potentiometric Detection, Electroanalysis 24 (2012) 146–152. https://doi.org/10.1002/elan.201100522.
[20] J. Cui, G. Lisak, S. Strzalkowska, J. Bobacka, Potentiometric sensing utilizing paper-based microfluidic sampling, Analyst 139 (2014) 2133–2136. https://doi.org/10.1039/c3an02157b.
[21] G. Lisak, J. Cui, J. Bobacka, Paper-based microfluidic sampling for potentiometric determination of ions, Sens. Actuators B Chem. 207 (2015) 933–939. https://doi.org/10.1016/j.snb.2014.07.044.
[22] K.M. Kelani, O.M. Badran, M.R. Rezk, M.R. Elghobashy, S.M. Eid, Widening the applications of the Just-Dip-It approach: a solid contact screen-printed ion-selective electrode for the real-time assessment of pharmaceutical dissolution testing in comparison to off-line HPLC analysis, RSC Adv. 11 (2021) 13366. https://doi.org/10.1039/d1ra00040c.
[23] M. Novell, M. Parrilla, G.A. Crespo, F.X. Rius, F.J. Andrade, Paper-Based Ion-Selective Potentiometric Sensors, Anal. Chem. 84 (2012) 4695–4702. https://doi.org/10.1021/ac202979j.
[24] W.J. Lan, X.U. Zou, M.M. Hamedi, J. Hu, C. Parolo, E.J. Maxwell, P. Bühlmann, G.M. Whitesides, Paper-Based Potentiometric Ion Sensing, Anal. Chem. 86 (2014) 9548–9553. https://doi.org/10.1021/ac5018088.
[25] M. Rostampour, D. Lawrence Jr, Z. Hamid, J. Darensbourg, P. Calvo-Marzal, K.Y. Chumbimuni-Torres, Highly Reproducible Flexible Ion-Selective Electrodes for the Detection of Sodium and Potassium in Artificial Sweat, Electroanalysis 34 (2022) 1–7. https://doi.org/10.1002/ELAN.202200121.
[26] M.L. Bouhoun, P. Blondeau, Y. Louafi, F.J. Andrade, A Paper-Based Potentiometric Platform for Determination of Water Hardness, Chemosensors 9 (2021). https://doi.org/10.3390/chemosensors9050096.
[27] R. Ding, N. Kumar Joon, A. Ahamed, A. Shafaat, M. Guzinski, M. Wagner, T. Ruzgas, J. Bobacka, G. Lisak, Gold-modified paper as microfluidic substrates with reduced biofouling in potentiometric ion sensing, Sens. Actuators B Chem. 344 (2021). https://doi.org/10.1016/j.snb.2021.130200.
[28] R. Ding, V. Krikstolaityte, G. Lisak, Inorganic salt modified paper substrates utilized in paper based microfluidic sampling for potentiometric determination of heavy

metals, Sens. Actuators B Chem. 290 (2019) 347–356. https://doi.org/10.1016/j.snb.2019.03.079.
[29] R. Silva, K. Zhao, R. Ding, W.P. Chan, M. Yang, J.S.Q. Yip, G. Lisak, Ion-selective membrane modified microfluidic paper-based solution sampling substrates for potentiometric heavy metal detection, R. Soc. Chem. 147 (2022) 4500–4509. https://doi.org/10.1039/d2an01108e.
[30] R. Ding, G. Lisak, Sponge-based microfluidic sampling for potentiometric ion sensing, Anal. Chim. Acta 1091 (2019) 103–111. https://doi.org/10.1016/j.aca.2019.09.024.
[31] R. Ding, Y.H. Cheong, K. Zhao, G. Lisak, Acidified paper substrates for microfluidic solution sampling integrated with potentiometric sensors for determination of heavy metals, Sens. Actuators B Chem. 347 (2021) 130567. https://doi.org/10.1016/J.SNB.2021.130567.
[32] G. Lisak, T. Arnebrant, T. Ruzgas, J. Bobacka, Textile-based sampling for potentiometric determination of ions, Anal. Chim. Acta 877 (2015) 71–79. https://doi.org/10.1016/j.aca.2015.03.045.
[33] R. Silva, A. Ahamed, Y.H. Cheong, K. Zhao, R. Ding, G. Lisak, Non-equilibrium potentiometric sensors integrated with metal modified paper-based microfluidic solution sampling substrates for determination of heavy metals in complex environmental samples, Anal. Chim. Acta 1197 (2022) 339495. https://doi.org/10.1016/j.aca.2022.339495.
[34] Y. Soda, E. Bakker, Ionic strength-independent potentiometric cation concentration sensing on paper using a tetrabutylammonium-based reference electrode, Sens. Actuators B Chem. 346 (2021) 130527. https://doi.org/10.1016/j.snb.2021.130527.
[35] R. Ding, M. Fiedoruk-Pogrebniak, M. Pokrzywnicka, R. Koncki, J. Bobacka, G. Lisak, Solid reference electrode integrated with paper-based microfluidics for potentiometric ion sensing, Sens. Actuators B Chem. 323 (2020) 128680. https://doi.org/10.1016/j.snb.2020.128680.
[36] A. Michalska, K. Maksymiuk, All-plastic, disposable, low detection limit ion-selective electrodes, Anal. Chim. Acta 523 (2004) 97–105. https://doi.org/10.1016/j.aca.2004.07.020.
[37] S.T. Mensah, Y. Gonzalez, P. Calvo-Marzal, K.Y. Chumbimuni-Torres, Nanomolar Detection Limits of Cd2+, Ag+, and K+ Using Paper-Strip Ion-Selective Electrodes, Anal. Chem. 86 (2014) 7269–7273. https://doi.org/10.1021/ac501470p.
[38] M. Rostampour, B. Bailey, C. Autrey, K. Ferrer, B. Vantoorenburg, P.K. Patel, P. Calvo-Marzal, K.Y. Chumbimuni-Torres, Single-Step Integration of Poly(3-Octylthiophene) and Single-Walled Carbon Nanotubes for Highly Reproducible Paper-Based Ion-Selective Electrodes, Anal. Chem. 93 (2021) 1271–1276. https://doi.org/10.1021/acs.analchem.0c04506.
[39] J. Kalisz, K. Węgrzyn, K. Maksymiuk, A. Michalska, 3D-Drawn Supports for Ion-Selective Electrodes, Anal. Chem. 95 (2022) 3436–3440. https://doi.org/10.1021/acs.analchem.1c05431.
[40] F.X. Rius-Ruiz, G.A. Crespo, D. Bejarano-Nosas, P. Blondeau, J. Riu, F.X. Rius, Potentiometric strip cell based on carbon nanotubes as transducer layer: Toward

low-cost decentralized measurements, Anal. Chem. 83 (2011) 8810–8815. https://doi.org/10.1021/ac202070r.
[41] S. Anastasova, A. Radu, G. Matzeu, C. Zuliani, U. Mattinen, J. Bobacka, D. Diamond, Disposable solid-contact ion-selective electrodes for environmental monitoring of lead with ppb limit-of-detection, Electrochimica Acta 73 (2012) 93–97. https://doi.org/10.1016/j.electacta.2011.10.089.
[42] M. Jendrlin, S. Khumngern, A. Numnuam, P. Thavarungkul, P. Kanatharana, D. Kirsanov, V.L. Zholobenko, L. Mendecki, A. Radu, Ion sensing pencil: Draw your own sensor, Sens. Actuators B Chem. 337 (2021) 129751. https://doi.org/10.1016/j.snb.2021.129751.
[43] M. Novell, T. Guinovart, P. Blondeau, F.X. Rius, F.J. Andrade, A paper-based potentiometric cell for decentralized monitoring of Li levels in whole blood, Lab. Chip 14 (2014) 1308–1314. https://doi.org/10.1039/c3lc51098k.
[44] S.M. Armas, A.J. Manhan, O. Younce, P. Calvo-Marzal, K.Y. Chumbimuni-Torres, Ready-to-use single-strip paper based sensor for multiplex ion detection, Sens. Actuators B Chem. 255 (2018) 1781–1787. https://doi.org/10.1016/j.snb.2017.08.194.
[45] F. Wang, Y. Liu, M. Zhang, F. Zhang, P. He, Home Detection Technique for Na + and K + in Urine Using a Self-Calibrated all-Solid-State Ion-Selective Electrode Array Based on Polystyrene−Au Ion-Sensing Nanocomposites, Anal. Chem. 93 (2021) 8318–8325. https://doi.org/10.1021/acs.analchem.1c01203.
[46] Q. An, S. Gan, J. Xu, Y. Bao, T. Wu, H. Kong, L. Zhong, Y. Ma, Z. Song, L. Niu, A multichannel electrochemical all-solid-state wearable potentiometric sensor for real-time sweat ion monitoring, Electrochem. Commun. 107 (2019) 106553. https://doi.org/10.1016/j.elecom.2019.106553.
[47] C. Jiang, X. Li, Y. Yao, Y. Ying, J. Ping, Fully Written Flexible Potentiometric Sensor Using Two-Dimensional Nanomaterial-Based Conductive Ink, Anal. Chem. 90 (2018) 13088–13095. https://doi.org/10.1021/acs.analchem.8b04334.
[48] A.H. Kamel, A.E.-G. Amr, A.A. Almehizia, E.A. Elsayed, G.O. Moustafa, Low-cost potentiometric paper-based analytical device based on newly synthesized macrocyclic pyrido-pentapeptide derivatives as novel ionophores for point-of-care copper(II) determination, RSC Adv. 11 (2021) 27174–27182. https://doi.org/10.1039/d1ra04712d.
[49] A.A. Almehizia, A.M. Naglah, M.G. Alanazi, A.E.-G.E. Amr, A.H. Kamel, Paper-Based Analytical Device Based on Potentiometric Transduction for Sensitive Determination of Phenobarbital, ACS Omega 8 (2023) 43538–43545. https://doi.org/10.1021/acsomega.3c03977.
[50] T. Ozer, I. Agir, C.S. Henry, Rapid prototyping of ion-selective electrodes using a low-cost 3D printed internet-of-things (IoT) controlled robot, Talanta 247 (2022) 123544. https://doi.org/10.1016/j.talanta.2022.123544.
[51] J. Wei, X. Zhang, S.M. Mugo, Q. Zhang, A Portable Sweat Sensor Based on Carbon Quantum Dots for Multiplex Detection of Cardiovascular Health Biomarkers, Anal. Chem. 94 (2022) 12772–12780. https://doi.org/10.1021/acs.analchem.2c02587.

[52] L. Mou, Y. Xia, X. Jiang, Epidermal Sensor for Potentiometric Analysis of Metabolite and Electrolyte, Anal. Chem. 93 (2022) 11525–11531. https://doi.org/10.1021/acs.analchem.1c01940.
[53] W.J. Lan, E.J. Maxwell, C. Parolo, D.K. Bwambok, A.B. Subramaniam, G.M. Whitesides, Paper-based electroanalytical devices with an integrated, stable reference electrode, Lab. Chip 13 (2013) 4103–4108. https://doi.org/10.1039/c3lc50771h.
[54] E. Carrilho, A.W. Martinez, G.M. Whitesides, Understanding Wax Printing: A Simple Micropatterning Process for Paper-Based Microfluidic, Anal. Chem. 81 (2009) 7091–7095. https://doi.org/10.1021/ac901071p.
[55] Y. Lu, W. Shi, L. Jiang, J. Qin, B. Lin, Rapid prototyping of paper-based microfluidics with wax for low-cost, portable bioassay, Electrophoresis 30 (2009) 1497–1500. https://doi.org/10.1002/elps.200800563.
[56] J.G. Bell, M.P.S. Mousavi, M.K. Abd El-Rahman, E.K.W. Tan, S. Homer-Vanniasinkam, G.M. Whitesides, Paper-based potentiometric sensing of free bilirubin in blood serum, Biosens. Bioelectron. 126 (2019) 115–121. https://doi.org/10.1016/j.bios.2018.10.055.
[57] D.L. Glasco, N.H.B. Ho, A.M. Mamaril, J.G. Bell, 3D Printed Ion-Selective Membranes and Their Translation into Point-of-Care Sensors, Anal. Chem. 93 (2021) 15826–15831. https://doi.org/10.1021/ACS.ANALCHEM.1C03762.
[58] J. Hu, A. Stein, P. Bühlmann, A Disposable Planar Paper-Based Potentiometric Ion-Sensing Platform, Angew. Chem. Int. Ed. 55 (2016) 7544–7547. https://doi.org/10.1002/anie.201603017.
[59] E.J. Herrero, P. Bühlmann, Potentiometric Sensors with Polymeric Sensing and Reference Membranes Fully Integrated into a Sample-Wicking Polyester Textile, Anal. Sens. 1 (2021) 188–195. https://doi.org/10.1002/ANSE.202100027.
[60] G. Xu, C. Cheng, W. Yuan, Z. Liu, L. Zhu, X. Li, Y. Lu, Z. Chen, J. Liu, Z. Cui, J. Liu, H. Men, Q. Liu, Smartphone-based battery-free and flexible electrochemical patch for calcium and chloride ions detections in biofluids, Sens. Actuators B Chem. 297 (2019) 126743. https://doi.org/10.1016/J.SNB.2019.126743.
[61] M.P.S. Mousavi, A. Ainla, E.K.W. Tan, M.K. Abd El-Rahman, Y. Yoshida, L. Yuan, H.H. Sigurslid, N. Arkan, M.C. Yip, C.K. Abrahamsson, S. Homer-Vanniasinkam, G.M. Whitesides, Ion sensing with thread-based potentiometric electrodes, Lab. Chip 18 (2018) 2279–2290. https://doi.org/10.1039/c8lc00352a.
[62] L. Wang, L. Wang, Y. Zhang, J. Pan, S. Li, X. Sun, B. Zhang, H. Peng, Weaving Sensing Fibers into Electrochemical Fabric for Real-Time Health Monitoring, Adv. Funct. Mater. 28 (2018) 1804456. https://doi.org/10.1002/ADFM.201804456.
[63] J. Hu, K.T. Ho, X.U. Zou, W.H. Smyrl, A. Stein, P. Bühlmann, All-Solid-State Reference Electrodes Based on Colloid-Imprinted Mesoporous Carbon and Their Application in Disposable Paper-based Potentiometric Sensing Devices, Anal. Chem. 87 (2015) 2981–2987. https://doi.org/10.1021/ac504556s.
[64] J. Hu, W. Zhao, P. Bühlmann, A. Stein, Paper-Based All-Solid-State Ion-Sensing Platform with a Solid Contact Comprising Colloid-Imprinted Mesoporous Carbon and a Redox Buffer, ACS Appl. Nano Mater. 1 (2018) 293–301. https://doi.org/10.1021/acsanm.7b00151.

[65] N. Ruecha, O. Chailapakul, K. Suzuki, D. Citterio, Fully Inkjet-Printed Paper-Based Potentiometric Ion-Sensing Devices, Anal. Chem. 89 (2017) 10608–10616. https://doi.org/10.1021/acs.analchem.7b03177.
[66] T. Zhang, A.M. Ratajczak, H. Chen, J.A. Terrell, C. Chen, A Step Forward for Smart Clothes-Fabric-Based Microfluidic Sensors for Wearable Health Monitoring, ACS Sens. 7 (2022) 3857–3866. https://doi.org/10.1021/acssensors.2c01827.
[67] T. Ozer, C.S. Henry, Microfluidic-based ion-selective thermoplastic electrode array for point-of-care detection of potassium and sodium ions, Michrochimica Acta 189 (2022) 152. https://doi.org/10.1007/s00604-022-05264-y.
[68] M. Parrilla, I. Ortiz-Gómez, R. Cánovas, A. Salinas-Castillo, M. Cuartero, G.A. Crespo, Wearable Potentiometric Ion Patch for On-Body Electrolyte Monitoring in Sweat: Toward a Validation Strategy to Ensure Physiological Relevance, Anal. Chem. 91 (2019) 8644–8651. https://doi.org/10.1021/acs.analchem.9b02126.
[69] W. Gao, S. Emaminejad, H.Y.Y. Nyein, S. Challa, K. Chen, A. Peck, H.M. Fahad, H. Ota, H. Shiraki, D. Kiriya, D.-H. Lien, G.A. Brooks, R.W. Davis, A. Javey, Fully integrated wearable sensor arrays for multiplexed in situ perspiration analysis, Nature 529 (2016) 509–514. https://doi.org/10.1038/nature16521.
[70] Q. Cao, B. Liang, X. Mao, J. Wei, T. Tu, L. Fang, X. Ye, A Smartwatch Integrated with a Paper-based Microfluidic Patch for Sweat Electrolytes Monitoring, Electroanalysis 33 (2021) 643–651. https://doi.org/10.1002/ELAN.202060025.
[71] M.N. Sweilam, S.F. Cordery, S. Totti, E.G. Velliou, P. Campagnolo, J.R. Varcoe, M.B. Delgado-Charro, C. Crean, Textile-based non-invasive lithium drug monitoring: A proof-of-concept study for wearable sensing, Biosens. Bioelectron. 150 (2020) 111897. https://doi.org/10.1016/j.bios.2019.111897.
[72] M.N. Sweilam, J.R. Varcoe, C. Crean, Fabrication and Optimization of Fiber-Based Lithium Sensor: A Step toward Wearable Sensors for Lithium Drug Monitoring in Interstitial Fluid, ACS Sens. 3 (2018) 1802–1810. https://doi.org/10.1021/acssensors.8b00528.
[73] T. Guinovart, G. Valdés-Ramírez, J.R. Windmiller, F.J. Andrade, J. Wang, Bandage-Based Wearable Potentiometric Sensor for Monitoring Wound pH, Electroanalysis 26 (2014) 1345–1353. https://doi.org/10.1002/elan.201300558.
[74] M. Parrilla, J. Ferré, T. Guinovart, F.J. Andrade, Wearable Potentiometric Sensors Based on Commercial Carbon Fibres for Monitoring Sodium in Sweat, Electroanalysis 28 (2016) 1267–1275. https://doi.org/10.1002/elan.201600070.
[75] R. Wang, Q. Zhai, Y. Zhao, T. An, S. Gong, Z. Guo, Q. Shi, Z. Yong, W. Cheng, Stretchable gold fiber-based wearable electrochemical sensor toward pH monitoring, J. Mater. Chem. B 8 (2020) 3655. https://doi.org/10.1039/c9tb02477h.
[76] T. Terse-Thakoor, M. Punjiya, Z. Matharu, B. Lyu, M. Ahmad, G.E. Giles, R. Owyeung, F. Alaimo, M. Shojaei Baghini, T.T. Brunyé, S. Sonkusale, Thread-based multiplexed sensor patch for real-time sweat monitoring, Flex. Electron. 4 (2020) 18. https://doi.org/10.1038/s41528-020-00081-w.
[77] B.S. Napier, G. Matzeu, M.L. Presti, F.G. Omenetto, Dry Spun, Bulk-Functionalized rGO Fibers for Textile Integrated Potentiometric Sensors, Adv. Mater. Technol. 7 (2021) 2101508. https://doi.org/10.1002/admt.202101508.

[78] K.J. Land, D.I. Boeras, X.S. Chen, A.R. Ramsay, R.W. Peeling, REASSURED diagnostics to inform disease control strategies, strengthen health systems and improve patient outcomes, Nat. Microbiol. 4 (2019) 46–54. https://doi.org/10.1038/s41564-018-0295-3.
[79] H. Gong, B. Ozgen, Fabric structures: Woven, knitted, or nonwoven, in: M. Miao, J.H. Xin (Eds.), Eng. High-Perform. Text., Woodhead Publishing, 2017: pp. 107–131. https://doi.org/10.1016/B978-0-08-101273-4.00007-X.
[80] J. Postlewaite, B. Lyon, S. Kalelkar, Cleanroom Wiper Applications for Removal of Surface Contamination, in: R. Kohli, K.L. Mittal (Eds.), Dev. Surf. Contam. Clean. Appl. Clean. Tech., Elsevier, 2013: pp. 555–564. https://doi.org/10.1016/b978-0-12-815577-6.00014-1.
[81] A. Michalska, M. Ocypa, K. Maksymiuk, Highly selective all-plastic, disposable, Cu2+-selective electrodes, Electroanalysis 17 (2005) 327–333. https://doi.org/10.1002/ELAN.200403107.
[82] J. Wang, L. Wang, G. Li, D. Yan, C. Liu, T. Xu, X. Zhang, Ultra-Small Wearable Flexible Biosensor for Continuous Sweat Analysis, ACS Sens. 7 (2022) 3102–3107. https://doi.org/10.1021/acssensors.2c01533.
[83] T. Guinovart, M. Parrilla, G.A. Crespo, F.X. Rius, F.J. Andrade, Potentiometric sensors using cotton yarns, carbon nanotubes and polymeric membranes, Analyst 138 (2013) 5208–5215. https://doi.org/10.1039/c3an00710c.
[84] E. Noviana, T. Ozer, C.S. Carrell, J.S. Link, C. McMahon, I. Jang, C.S. Henry, Microfluidic Paper-Based Analytical Devices: From Design to Applications, Chem. Rev. 121 (2021) 11835–11885. https://doi.org/10.1021/acs.chemrev.0c01335.
[85] R. Ding, Y.H. Cheong, A. Ahamed, G. Lisak, Heavy Metals Detection with Paper-Based Electrochemical Sensors, Anal. Chem. 93 (2021) 1880–1888. https://doi.org/10.1021/acs.analchem.0c04247.
[86] F. Arduini, Electrochemical paper-based devices: When the simple replacement of the support to print ecodesigned electrodes radically improves the features of the electrochemical devices, Curr. Opin. Electrochem. 35 (2022) 1–8. https://doi.org/10.1016/j.coelec.2022.101090.
[87] M. Cuartero, M. Parrilla, G.A. Crespo, Wearable potentiometric sensors for medical applications, Sensors 19 (2019) 1–24. https://doi.org/10.3390/s19020363.
[88] M.-Y. Choi, M. Lee, J.-H. Kim, S. Kim, J. Choi, J.-H. So, H.-J. Koo, A fully textile-based skin pH sensor, J. Ind. Text. 51 (2022) 441S-457S. https://doi.org/10.1177/15280837211073361.
[89] J. Militky, The Chemistry, Manufacture and Tensile Behavior of Polyester Fabrics, in: A.R. Bunsell (Ed.), Handb. Tensile Prop. Text. Tech. Fibers, Woodhead Publishing, New York, 2009: pp. 223–314.
[90] J. Xu, Z. Zhang, S. Gan, H. Gao, H. Kong, Z. Song, X. Ge, Y. Bao, L. Niu, Highly Stretchable Fiber-Based Potentiometric Ion Sensors for Multichannel Real-Time Analysis of Human Sweat, ACS Sens. 5 (2020) 2834–2842. https://doi.org/10.1021/acssensors.0c00960.
[91] W.E. Morf, The Principles of Ion-Selective Electrodes and of Membrane Transport, Elsevier Science, New York, 1981.

[92] P.C. Meier, Two Parameter Debye-Hückel Approximation for the Evaluation of Mean Activity Coefficients of 109 Electrolytes, Anal. Chim. Acta 136 (1982) 363–368.
[93] Z. Szigeti, T. Vigassy, E. Bakker, E. Pretsch, Approaches to improving the lower detection limit of polymeric membrane ion-selective electrodes, Electroanalysis 18 (2006) 1254–1265. https://doi.org/10.1002/elan.200603539.
[94] E. Jaworska, G. Pomarico, B. Berionni Berna, K. Maksymiuk, R. Paolesse, A. Michalska, All-solid-state paper based potentiometric potassium sensors containing cobalt(II) porphyrin/cobalt(III) corrole in the transducer layer, Sens. Actuators B Chem. 277 (2018) 306–311. https://doi.org/10.1016/j.snb.2018.08.090.
[95] E.J. Herrero, B.K. Troudt, P. Bühlmann, The Effect of Paper on the Detection Limit of Paper-Based Potentiometric Chloride Sensors, Anal. Chem. 94 (2022) 14898–14905. https://doi.org/10.1021/acs.analchem.2c02261.
[96] M. Rich, L. Mendecki, S.T. Mensah, E. Blanco-Martinez, S. Armas, P. Calvo-Marzal, A. Radu, K.Y. Chumbimuni-Torres, Circumventing Traditional Conditioning Protocols in Polymer Membrane-Based Ion-Selective Electrodes, Anal. Chem. 88 (2016) 8404–8408. https://doi.org/10.1021/acs.analchem.6b01542.
[97] Laboratory Requirements, in: US Code Fed. Regul. 493931, US Code of Federal Regulations 493.931, 2003.
[98] A.M. Yehia, M.A. Farag, M.A. Tantawy, A novel trimodal system on a paper-based microfluidic device for on-site detection of the date rape drug “ketamine,” Anal. Chim. Acta 1104 (2020) 95–104. https://doi.org/10.1016/j.aca.2020.01.002.
[99] R. Vinoth, T. Nakagawa, J. Mathiyarasu, A.M.V. Mohan, Fully Printed Wearable Microfluidic Devices for High-Throughput Sweat Sampling and Multiplexed Electrochemical Analysis, ACS Sens. 6 (2021) 1174–1186. https://doi.org/10.1021/acssensors.0c02446.
[100] J. Ping, Y. Wang, K. Fan, W. Tang, J. Wu, Y. Ying, High-performance flexible potentiometric sensing devices using free-standing graphene paper, J. Mater. Chem. B 1 (2013) 4781. https://doi.org/10.1039/c3tb20664e.
[101] E.J. Herrero, T. Goto, P. Bühlmann, Hydrophilic redox buffers for textile-based potentiometric sensors, Sens. Actuators B Chem. 408 (2024) 135527. https://doi.org/10.1016/j.snb.2024.135527.
[102] X.V. Zhen, C.R. Rousseau, P. Bühlmann, Redox Buffer Capacity of Ion-Selective Electrode Solid Contacts Doped with Organometallic Complexes, Anal. Chem. 90 (2018) 11000–11007. https://doi.org/10.1021/acs.analchem.8b02595.
[103] Y.H. Cheong, L. Ge, N. Zhao, L. Kuan Teh, G. Lisak, Ion selective electrodes utilizing a ferrocyanide doped redox active screen-printed solid contact-impact of electrode response to conditioning, J. Electroanal. Chem. 870 (2020). https://doi.org/10.1016/j.jelechem.2020.114262.
[104] U. Vanamo, J. Bobacka, Instrument-free control of the standard potential of potentiometric solid-contact ion-selective electrodes by short-circuiting with a conventional reference electrode, Anal. Chem. 86 (2014) 10540–10545. https://doi.org/10.1021/ac501464s.
[105] R.P. Buck, E. Lindner, Recomendations for Nomenclature of Ion-Selective Electrodes, Pure Appl. Chem. 66 (1994) 2527–2536.

[106] P. Bühlmann, E. Pretsch, E. Bakker, Carrier-based ion-selective electrodes and bulk optodes. 2. Ionophores for potentiometric and optical sensors, Chem. Rev. 98 (1998) 1593–1688. https://doi.org/10.1021/cr970113+.